

Inhaltsverzeichnis

1	Introduction	3
1.1	FAIR project	3
1.2	Beam transfer systems of the FAIR accelerator	3
2	Theoretical background	4
2.1	Introduction of the bunch to bucket transfer	4
2.1.1	Phase difference between two RF systems	5
2.1.2	Synchronization of two RF systems	5
2.1.2.1	Phase shift method	6
2.1.2.1.1	Radial excursion and momentum shift due to frequency modulation	7
2.1.2.1.2	Transverse dynamics analysis	7
2.1.2.1.3	Shift of synchronous phase	7
2.1.2.1.4	Bucket area factor	8
2.1.2.1.5	Adiabaticity analysis	8
2.1.2.1.6	$d\phi_s(t)/dt$	9
2.1.2.2	Examples of RF frequency modulation for 200Mev U^{28+} SIS18	9
2.1.2.3	Frequency beating method	9
2.1.2.3.1	Longitudinal dynamics analysis	10
2.1.2.4	Example of frequency beating method for SIS18 and SIS100 1 Seite	10
2.1.2.4.1	Frequency beating method for SIS18 and ESR 2-3 Seiten	11
2.1.3	Bucket label	12
2.1.4	Synchronization of the extraction and injection kicker	12
2.1.5	Beam indication for the beam instrumentation	14
2.2	Prerequisites/boundary conditions for the B2B transfer system	14
2.2.1	FAIR control system	14
2.2.1.1	BuTiS	14
2.2.1.2	GMT	15
2.2.1.3	FESA	15
2.2.1.4	SM	16
2.2.2	LLRF system	16
3	First idea on the B2B transfer system	19
3.1	Data acquisition from two synchrotrons	19
3.2	Coarse synchronization	19

3.3	Fine synchronization	19
4	Concept of the B2B transfer system	20
4.1	Basic procedure of the B2B transfer system for FAIR	20
4.2	Functional blocks and responsibilities	20
5	Realization and systematic investigation of the B2B transfer system	23
5.1	Investigation from the beam dynamics view for two synchronization methods of U^{28+} for SIS18	23
5.1.1	Longitudinal dynamic analysis for the simulation	24
5.1.2	Transverse dynamics analysis for the simulations	27
5.1.3	Longitudinal dynamics analysis of the frequency beating for SIS18	28
5.2	GMT systematic investigation for the B2B transfer system	29
5.2.1	Calculation of the synchronization window and its uncertainty	29
5.2.1.1	Synchronization window for the phase shift method and its uncertainty	30
5.2.1.2	Synchronization window for the frequency beating method and its uncertainty	32
5.2.2	WR network latency measurement	34
5.3	Kicker systematic investigation for the B2B transfer system	36
5.3.1	SIS18 extraction kicker units	36
5.3.2	SIS100 injection kicker units	38
5.4	Test setup for the data collection, merging and redistribution of the B2B transfer system	39
5.4.1	Test requirement	39
5.4.2	Test setup introduction	39
5.4.3	Test result	41
6	Existing transfer system and the transfer system of the FAIR accelerators	43
6.1	Existing transfer from SIS18 to ESR	43
6.2	B2B transfer from SIS18 to ESR to CRYRING	43
7	Summary	44
8	Acknowledgement	45
9	References	46

Kapitel 1

Introduction

1.1 FAIR project

1.2 Beam transfer systems of the FAIR accelerator

Kapitel 2

Theoretical background

2.1 Introduction of the bunch to bucket transfer

- Energy match

The 'magnetic rigidity' of a beam is defined as the following:

$$B\rho = \frac{p}{e} \quad (2.1)$$

where p is the magnitude of the particle momentum, e is the charge of the particle, B is magnetic field, and ρ is the bending radius of a particle immersed in a magnetic field B. The ratio of p to e describes the 'stiffness' of a beam, it can be considered as a measure of how much angular deflection results when a particle travels through a given magnetic field.

The bunch is transferred from the source to the target machine with the same energy. So the beam has the same momentum and velocity for both machines. According to eq. 2.1, the magnetic rigidity of two machines must be matched:

$$B_{src}\rho_{src} = B_{trg}\rho_{trg} \quad (2.2)$$

Besides, the rf frequency of two machines must meet the following relation.

$$C_{src} \frac{f_{rf}^{src}}{h^{src}} = \beta c = C_{trg} \frac{f_{rf}^{trg}}{h^{trg}} \quad (2.3)$$

- RF synchronization

For the proper B2B transfer, the phase advance between the bunch and the bucket must be precisely controlled before the bunch is ejected. The process of achieving the detailed phase adjustment is termed "synchronization".

$$\frac{f_{rf}^{src}}{f_{rf}^{trg}} = \frac{C_{trg}h^{src}}{C_{src}h^{trg}} \quad (2.4)$$

The synchronization can be achieved by an azimuthal positioning of the bunch in the source machine or the bucket in the target machine. This is so-called "phase shift method". When two rf frequencies are slightly different, they are beating, perceived as periodic variations in phase difference whose rate is the difference between the two frequencies. The synchronization can be automatically achieved. This is so-called "frequency beating method".

- Bucket synchronization

Fast extraction can only proceed when the required bucket comes. The extraction must be correctly synchronized with respect to a reference signal at the following frequency, which is called bucket marker.

$$\frac{f_{rf}^{src}}{p} = \frac{f_{rf}^{trg}}{q} \quad (2.5)$$

- Extraction and injection synchronization

Bunch fast extraction must happen exactly one "time of flight" before the required bucket of the target machine passes the injection region. The injection kicker must kick when the bucket passes the injection region.

$$t_{ext}^{src} + t_{tof} = t_{inj}^{trg} \quad (2.6)$$

2.1.1 Phase difference between two RF systems

For the RF synchronization between two machines, the first step is to measure the phase difference between two RF systems.

2.1.2 Synchronization of two RF systems

The B2B transfer means that one bunch of particles, circulating inside the source synchrotron, is transferred into the center of a bucket of the target synchrotron. For the proper transfer, the phase advance between the bunch and the bucket must be precisely controlled before the bunch is ejected. The process of achieving the detailed phase adjustment is usually named as "synchronization". There are usually two methods available for the synchronization process, the phase shift method and the frequency beating method. Both methods provide a time frame for the B2B transfer, within which a bunch could be transferred into a bucket with the center mismatch at least better than 1° . The time frame is called the synchronization window.

For both methods, the accompanying beam dynamics must be taken into consideration. Of the four variables, the revolution frequency $f(t)$, the bending magnetic-field $B(t)$, the momentum of particle $p(t)$ and the orbit radius $R(t)$, only two are independent. This leads to four very useful differential relations. The momentum of particle is given by

$$p(t) = e\rho_0 \left[\frac{R(t)}{R_0} \right]^{1/\alpha_p} B(t) \quad (2.7)$$

where e is the charge of particle; ρ_0 , the nominal bending radius; R_0 , its nominal value; ; and α_p , the momentum compaction factor. From eq. 2.7, the first-order total differential of $p(t)$ is given as

$$dp(t) = \frac{e\rho_0}{\alpha_p(R_0)^{1/\alpha_p}} B(t) R(t)^{1/\alpha_p - 1} dR(t) + e\rho_0 \left[\frac{R(t)}{R_0} \right]^{1/\alpha_p} B(t) dB(t) \quad (2.8)$$

Dividing both sides of eq. 2.8 by $p(t)$, we obtain

$$\frac{dp(t)}{p(t)} = \gamma_t^2 \frac{\Delta R}{R} + \frac{\Delta B}{B} \quad (2.9)$$

Now, for circular accelerators, the following general relation holds

$$f(t) = \frac{v(t)}{2\pi R(t)} \quad (2.10)$$

where $v(t)$ is its velocity. The total differential of $f(t)$ is given by

$$df(t) = \frac{1}{2\pi} \left[\frac{dv(t)}{R(t)} - \frac{v(t)}{R^2(t)} dR(t) \right] \quad (2.11)$$

Dividing both sides of eq. 2.11 by $f(t)$ yields

$$\frac{df(t)}{f(t)} = \frac{dv(t)}{v(t)} - \frac{dR(t)}{R(t)} \quad (2.12)$$

The fractional change in $v(t)$ is related to the fractional change in $p(t)$:

$$\frac{dp(t)}{p(t)} = \gamma^2(t) \frac{dv(t)}{v(t)} \quad (2.13)$$

where $\gamma(t)$ is the relativistic factor, which measures the total particle energy, $E(t)$, in units of the particle rest energy, E_0 . Solving $dv(t)/v(t)$ from eq. 2.13 and substituting it into eq. 2.12 yields

$$\frac{df(t)}{f(t)} = \gamma^2(t) \frac{dp(t)}{p(t)} - \frac{dR(t)}{R(t)} \quad (2.14)$$

Replacing $dp(t)/p(t)$ in eq. 2.14 with eq. 2.9, we have

$$\frac{df(t)}{f(t)} = \gamma^2(t) \frac{dB(t)}{B(t)} + \left[\frac{\gamma_t^2}{\gamma^2(t)} - 1 \right] \frac{dR(t)}{R(t)} \quad (2.15)$$

where γ_t is the transition gamma, which is related to α_p as $\gamma_t = 1/\sqrt{\alpha_p}$. In the same way, solving $dR(t)/R(t)$ from eq. 2.9 and substituting it into eq. 2.14, we obtain

$$\frac{df(t)}{f(t)} = \left(\frac{1}{\gamma^2(t)} - \frac{1}{\gamma_t^2} \right) \frac{dp(t)}{p(t)} + \frac{1}{\gamma_t^2} \frac{dB(t)}{B(t)} \quad (2.16)$$

2.1.2.1 Phase shift method

At a scheduled time well before ejection, the phase advance between the beam in the source synchrotron and a reference bucket in the target synchrotron are measured with respect to the phase of a common Synchronization Reference Signal, which is synchronously distributed to the source and target synchrotrons. Based on the measured phase advance, the Reference Radio Frequency (RF) Signals of the source or target or both synchrotrons are modulated away from their nominal value for a period of time and then modulated back so that the phase shift created by the frequency modulation could compensate for the expected phase difference. After the phase shift, the bunches of the source synchrotron are synchronized with the buckets of the target synchrotron. The phase shift process must be performed adiabatically for the longitudinal emittance to be preserved.

Fig. 1 shows the synchronization window for the phase shift method. The top and bottom RF signals are respectively from the source and target synchrotrons.

For the phase shift method two RF signals are of the same frequency. The blue dots show the position of the bunches of the source synchrotron, the red dots correspond to the bucket positions of the target synchrotron. The compensation of the time-of-flight is not drawn here. The red dashed line shows the end of the phase shift process and the beginning of the synchronization window, drawn in yellow. After the phase shift, bunches match with the corresponding buckets.

A particular case of the B2B synchronization occurs, when the target synchrotron is empty, i.e. it did not capture any bunch yet, the phase shift can be done for the target synchrotron without adiabatical consideration (e.g. Phase jump is possible).

2.1.2.1.1 Radial excursion and momentum shift due to frequency modulation

For the phase shift method, the magnetic field is not affected by the frequency modulation, so $\Delta B = 0$. By substituting $\Delta B = 0$ into eq. 2.15 and eq. 2.16, we could get respectively the accompanying radial excursion and momentum shift by the frequency modulation.

$$\frac{\Delta f}{f} = \left(\frac{\gamma_t^2}{\gamma^2} - 1 \right) \frac{\Delta R}{R} \quad (2.17)$$

and

$$\frac{\Delta f}{f} = \left(\frac{1}{\gamma^2} - \frac{1}{\gamma_t^2} \right) \frac{\Delta p}{p} \quad (2.18)$$

2.1.2.1.2 Transverse dynamics analysis

The momentum spread $\Delta p/p \neq 0$ during the phase shift process causes chromaticity drift ΔQ . Q' is the chromaticity.

$$\Delta Q = Q' \frac{\Delta p}{p} \quad (2.19)$$

2.1.2.1.3 Shift of synchronous phase

The synchronous phase deviates from 0° during the frequency modulation. From the expression of the particle momentum, $p(t)$, given in eq. 2.7, the time derivative of $p(t)$ can be written as

$$\frac{dp(t)}{dt} = \frac{e\rho_0 B(t)}{\alpha_p R_0^{1/\alpha_p}} R(t)^{1/\alpha_p - 1} \frac{dR(t)}{dt} + e\rho_0 \left(\frac{R(t)}{R_0} \right)^{1/\alpha_p} \frac{dB(t)}{dt} \quad (2.20)$$

Now, the relationship between the rate of change in momentum of a particle, $dp(t)/dt$, and the force applied on it, $F(t)$, is governed by Newton's second law:

$$\frac{dp(t)}{dt} = F(t) \quad (2.21)$$

$F(t)$ is given by the product of the accelerating electric field, $E(t)$, and the charge of particle, e . Substituting $dp(t)/dt$ given in eq. 2.20 and $F(t) = eE(t)$ into eq. 2.21, we have

$$\frac{e\rho_0 B(t)}{\alpha_p R_0^{1/\alpha_p}} R(t)^{1/\alpha_p - 1} \frac{dR(t)}{dt} + e\rho_0 \left(\frac{R(t)}{R_0} \right)^{1/\alpha_p} \frac{dB(t)}{dt} = eE(t) \quad (2.22)$$

From this equation, we obtain the expression of energy gain in one turn,

$$2\pi R_0 \left[\frac{e\rho_0 B(t)}{\alpha_p R_0^{1/\alpha_p}} R(t)^{1/\alpha_p - 1} \frac{dR(t)}{dt} + e\rho_0 \left(\frac{R(t)}{R_0} \right)^{1/\alpha_p} \frac{dB(t)}{dt} \right] = eV(t) \sin[\phi_{s0}(t) + \Delta\phi_s(t)] \quad (2.23)$$

where $V(t)$ is the RF accelerating voltage per turn; ϕ_{s0} , the synchronous phase in the operation with no frequency modulation; and $\phi_s(t)$, the change in the synchronous phase originating from the rf frequency modulation.

The magnetic field is not affected by the frequency change, we can assume $dB(t)/dt = 0$. Before the synchronization, it is a stationary bucket with the synchronous phase 0° . Then, eq. 2.23 reduce to

$$2\pi R_0 \left[\frac{e\rho_0 B(t)}{\alpha_p R_0^{1/\alpha_p}} R(t)^{1/\alpha_p - 1} \frac{dR(t)}{dt} \right] = eV(t) \sin[\Delta\phi_s(t)] \quad (2.24)$$

Solving $\Delta\phi_s(t)$ from eq. 2.24, we have

$$\Delta\phi_s(t) = \sin^{-1} \left[\frac{2\pi\rho_0 B(t)}{\alpha_p V} \left(\frac{R(t)}{R_0} \right)^{1/\alpha_p - 1} \frac{dR(t)}{dt} \right] \quad (2.25)$$

From eq. 2.25, we know that $\Delta\phi_s(t)$ is only determined by $dR(t)/dt$ during the frequency modulation.

2.1.2.1.4 Bucket area factor

At the flattop, the bucket is a stationary bucket with $\phi_s(t) = 0$. During the frequency modulation process, the bucket becomes a running bucket with $\Delta\phi_s(t) \neq 0$. The ratio of bucket areas of a running bucket to a stationary bucket is bucket area factor $\alpha(\Delta\phi_s)$. During the rf frequency modulation, the bucket area factor during the frequency modulation should be bigger than 80% in order for bunches to be preserved. The bucket area factor could be estimated by [13]

$$\alpha_b(\Delta\phi_s) \approx (1 - \sin(\Delta\phi_s))(1 + \sin(\Delta\phi_s)) \quad (2.26)$$

2.1.2.1.5 Adiabaticity analysis

$\omega_s(t)$ is the small-amplitude synchrotron frequency given by

$$\omega_s(t) = \left[-\frac{\eta(t) h \omega_{rev}^2(t) e V(t) \cos \phi_s(t)}{2\pi \beta^2(t) E(t)} \right]^{1/2} \quad (2.27)$$

A process is called “adiabatic” when the RF parameters are changed slowly enough for the longitudinal emittance to be preserved. The condition that the parameters are slowly varying can be expressed by

$$\varepsilon = \frac{1}{\omega_s^2(t)} \left| \frac{d\omega_s(t)}{dt} \right| \ll 1 \quad (2.28)$$

Compared with $\phi_s(t)$, all of the other variables change very slowly. $\phi_s(t) = \phi_{s0}(t) + \Delta\phi_s(t)$. $\phi_{s0}(t)$ is the synchronous phase in the operation with no frequency modulation, and $\Delta\phi_s(t)$ is the change in the synchronous phase, which originates

from the frequency modulation. From Eq. (??) and Eq. (2.27), we can write the adiabaticity parameter ε , as follows:

$$\varepsilon \approx \frac{1}{2\omega_{s0}(t)} |\tan\phi_s(t) \frac{d\phi_s(t)}{dt}| \quad (2.29)$$

Eq. (2.29) clearly shows that $\phi_s(t)$ and $d\phi_s(t)/dt$ play important roles for the adiabaticity when the frequency is modulated. Now let us deduce the the frequency requirement corresponding to these two factors.

substituting Eq. (??) into Eq. (??)

$$V \sin\phi_s = \frac{2\pi R_0 \rho B}{(\frac{1}{\gamma}^2 - \frac{1}{\gamma_t}^2)} \frac{\dot{f}}{f} \quad (2.30)$$

The bucket area factor is determined by the synchronous phase change $\Delta\phi_s$. Based on Eq. (2.31), we know that \dot{f} is important for the bucket size.

2.1.2.1.6 $d\phi_s(t)/dt$

$$V \cos\phi_s \frac{d\phi_s}{dt} = \frac{2\pi R_0 \rho B}{(\frac{1}{\gamma}^2 - \frac{1}{\gamma_t}^2)} \frac{\ddot{f}}{f} \quad (2.31)$$

Based on the adiabaticity Eq. (2.28), $d\phi_s(t)/dt$ must be existing. So \ddot{f} must be existing. It means that \dot{f} must be continuous.

2.1.2.2 Examples of RF frequency modulation for 200Mev U^{28+} SIS18

To achieve a required phase shift, the RF frequency is modulated away from that required by the bending magnetic field. Let $\Delta\phi$ be the phase shift to be achieved and $\Delta f_{rf}(t)$ the RF frequency variation to accomplish it; then,

$$\Delta\phi = 2\pi \int_{t_0}^{t_0+T} \Delta f_{rf}(t) dt \quad (2.32)$$

where T is the period of frequency modulation and t_0 is the time at which the modulation begins.

We have to introduce a phase shift of up to $\pm\pi$ [rad] in the RF phase. This is the worstcase scenario, and in practice, the phase shift might be much less. We consider here the following four examples of frequency modulation; simple frequency-offset modulation (Case (1)), triangular modulation (Case (2)), sinusoidal modulation (Case (3)) and parabola modulation (Case (4)), (see Fig. ??(a)).Here we make use of the maximum \dot{f} 64 Hz/ms during the 1st stage of rf ramp to guarantee the 90% bucket area factor.

2.1.2.3 Frequency beating method

The frequency beating method uses the effect of two RF signals of slightly different frequencies, perceived as periodic variations in phase difference whose rate is the difference between the two frequencies. The RF frequency of the source or the target or both synchrotrons is detuned long before the ejection, then the difference between the phase of the bunch/bucket and the phase of the Synchronization Reference Signal

is measured. Based on the measured phase, the synchronization is realized when the phase difference of the two RF frequencies corresponds to the ideal phase difference ($\Delta\theta = 0^\circ$). The $\Delta\theta$ is the mismatch between the bunch center and the corresponding bucket center. Because of the slightly different RF frequencies, a mismatch between the bunch and bucket centers exists. In principle, the B2B transfer requirement for FAIR allows a bunch to bucket center mismatch of 1° , which brings a symmetric time frame with respect to the time of the ideal phase difference, resulting in the maximum synchronization window for the frequency beating method, drawn in yellow (see Fig. 2). The compensation of the time-of-flight is not drawn. The red dashed line shows the time for the expected phase difference. During the detune process, the magnetic field and radius excursion react and the momentum is not affected.

2.1.2.3.1 Longitudinal dynamics analysis

For the frequency beating method, we guarantee the extraction and injection energy always match, which means that the momentum is not affected by the frequency change, namely $\Delta p = 0$; then the general relation between the radial excursion and RF frequency change Eq. (??) reduces to Eq. (2.38) and the general relation between the magnetic field change and RF frequency change Eq. (2.9) reduces to Eq. (2.39).

$$\frac{\Delta f}{f} = -\frac{\Delta R}{R} \quad (2.33)$$

$$\frac{\Delta f}{f} = \frac{1}{\gamma_t^2} \times \frac{\Delta B}{B} \quad (2.34)$$

2.1.2.4 Example of frequency beating method for SIS18 and SIS100 1 Seite

Because the circumference ratio of the large machine to the small machine is a perfect integer, the rf frequency at the flattop of SIS18 is same as that of SIS100. So the first step for the bunch to bucket transfer is the RF frequency de-tune. In order to realize the frequency beating between two synchrotrons, the RF frequency of the source synchrotron or the target synchrotron or both synchrotrons can be de-tuned. It means that the particles on the de-tuned synchrotron run at an average radius different by ΔR from the designed orbit R . For the synchronization of the SIS18 and the SIS100, we will de-tune the RF frequency on the SIS18. The SIS18 operates with a cycle length of 520ms, harmonic number of 2 ($h = 2$), and RF frequency of approximately 0.43 MHz at injection and approximately 1.57 MHz at ejection for the U^{28+} [10]. During nominal operation, the SIS18 forms two bunches from the beam injected at $11.4 \text{ MeV}/\mu$ and accelerates them up to $200 \text{ MeV}/\mu$. From the SIS18, 4 batches, each of 2 bunches, are transferred at maximum 10ms intervals to the SIS100. The harmonic number of the SIS100 is 10 and the SIS100 RF frequency is fixed at approximately 1.57 MHz during the injection period to simplify the RF control system and to avoid perturbing batches already transferred.

This RF frequency de-tune is done accompanying with the RF ramp. Accepting

to decentre the orbit by 8mm for the SIS18 [7]:

$$\frac{\Delta R}{R} \approx 2.4 \times 10^{-4} \quad (2.35)$$

We know the basic differential relations among the fractional change in the RF frequency f , the fractional change in the momentum p , the fractional change in the bending magnetic field B and the fractional change in the radius R as follows [8].

$$\frac{\Delta f}{f} = \frac{1}{\gamma^2} \frac{\Delta p}{p} - \frac{\Delta R}{R} \quad (2.36)$$

$$\frac{\Delta f}{f} = \left(\frac{1}{\gamma^2} - \frac{1}{\gamma_t^2} \right) \frac{\Delta p}{p} + \frac{1}{\gamma_t^2} \frac{\Delta B}{B} \quad (2.37)$$

where γ is the relativistic factor, which measures the total particle energy, E , in units of the particle rest energy, E_0 ; γ_t is the transition gamma; Δf and ΔB are the frequency and bending magnetic field deviation for the frequency de-tune; Δp is the momentum deviation.

In our case of the frequency beating method, we guarantee the extraction and injection energy always match, which means that the momentum is not affected by the frequency change, namely $\Delta p = 0$; then the general relation between the radial excursion and RF frequency change Eq. (2.36) reduces to Eq. (2.38) and the general relation between the magnetic field change and RF frequency change Eq. (2.37) reduces to Eq. (2.39).

$$\frac{\Delta f}{f} = -\frac{\Delta R}{R} \quad (2.38)$$

$$\frac{\Delta f}{f} = \frac{1}{\gamma_t^2} \times \frac{\Delta B}{B} \quad (2.39)$$

From these equations, the RF frequency and the magnetic field change at the U^{28+} extraction energy 200MeV/u [7] ($\gamma_t = 5.8$) are

$$\frac{\Delta f}{f} = -2.4 \times 10^{-4} \quad (2.40)$$

$$\frac{\Delta B}{B} = -8.1 \times 10^{-3} \quad (2.41)$$

where the maximum RF frequency de-tune is approximate to 370 Hz at 1.57 MHz for the U^{28+} . In this paper, we assume Rf frequency de-tune for the SIS18 equals to 200 Hz for the sake of simplicity. The beating period is 5ms.

2.1.2.4.1 Frequency beating method for SIS18 and ESR 2-3 Seiten

Because the circumference ratio of the ESR injection orbit to the SIS18 designed orbit is not a perfect integer, two machines begin beating automatically. He

2.1.3 Bucket label

After synchronization, the bunch is synchronized to an arbitrary RF bucket. For the proper injection, we must know which buckets are already filled and which buckets should be filled by next injection cycle. So a reproduced signal at the target revolution frequency is used as the bucket marker, which labels bucket 1 of the target synchrotron. The SM knows the bucket pattern and a proper bucket offset will be applied on each injection cycle to the bucket marker.

2.1.4 Synchronization of the extraction and injection kicker

For the proper B2B transfer, the extraction and injection kickers must be synchronized with the beam. Because the beam of two rings are synchronized with each other, the extraction and injection are synchronized indirectly. Thyratrons are used for kicker systems at FAIR accelerator.

- Extraction kicker

Here we discuss that all bunches are extracted by one time extraction kick. The flattop is at least one revolution period. The fall time is not constrained. If there is no empty RF bucket of the ring, the rise time of the extraction kicker must be shorter than the bunch gap. If there is at least one empty RF bucket, the rise of the magnetic field could be achieved within the gap of the empty RF buckets.

- Injectin kicker

For multi-batch injection, the rise time of the injection kicker must be shorter than the bunch gap. The flattop is determined by the length of the bunches to be injected. If all buckets must be filled, the fall time must be shorter than the bunch gap. If at least one bucket is kept empty, the fall of the magnetic field could be achieved within the gap of the empty RF buckets. If the ring needs only one time injection, the rise time is not constrained. The flattop determined by the length of the bunches to be injected. The fall time must be shorter than the bunch gap or the gap of the empty RF buckets.

For FAIR project, there are several different type of kicker system. Here we introduce SIS18 extraction, SIS100 injection and extracion/emergency kicker system.

The SIS100 extraction kicker system is used for the regular extraction and the emergency extraction by bipolar operation. It consists of eight kicker magnets. Each magnet is placed between the two cable capacitors. Both cable capacitors will be charged at the same time with a high voltage DC power supply. The polarity of the magnetic field changes with the direction of the discharge current, which are controled by two thyratron switches. One polarity directs the beam into the extraction channel, the other polarity directs the beam into an underground beam dump for an emergency case. The system produces rectangular pulses with different polarities of the kicker field.

The SIS18 extraction and SIS100 injection kicker have the monopolar operation. Two cable capacitors will be charged at the same time with a high voltage DC power supply. By closing the main switch the capacitor is being discharged via the kicker magnet, which produces a rectangular kicker pulse. The pulse length can be modified by closing the dump switch in correlation with the main switch.

Fig. 2.1 shows the synchronization of the SIS18 extraction and SIS100 injection kicker for U^{28+} B2B transfer. Four batches of U^{28+} at 200 MeV/u are injected into eight out of ten buckets of SIS100. Each batch consists of two bunches. The 9th and 10th bucket may be used as bunch gap for the emergency kick. The SIS18 revolution frequency marker and SIS100 bucket markers represent time when the SIS18 bunch 1 (1st) and SIS100 bucket 1 (#1) passes by the virtual RF cavity, which is a virtual position in the synchrotron to which the Reference RF Signal corresponds. In Fig. 2.1, the numbers correspond to the consideration of following factors for the synchronization:

- Bucket pattern ($delay_{bucket}$. E.g. $delay_{bucket}$ = One SIS18 revolution period. Bucket 3 and 4 will be filled)
- Compensation of Time-of-flight (TOF)
- Distance between the virtual RF cavity and the extraction/injection position (t_{src} and t_{trg}).
- Extraction and injection kicker delays (D_{ext} and D_{inj})

After the synchronization, the phase difference between the SIS18 and the SIS100 revolution frequency markers equals to the sum of t_{src} , t_{trg} and TOF. The extraction kicker will be triggered by the extraction kick delay compensation, $Th=1SIS1\ 00 + Th=1SIS18 - TOF - t_{trg} - D_{ext}$ and the injection kicker will be triggered by the injection kick delay compensation, $Th=1SIS1\ 00 + Th=1SIS1\ 8 - t_{trg} - D_{inj}$. See Fig. 9. Both extraction and injection kick delay compensation values are provided by the SM.

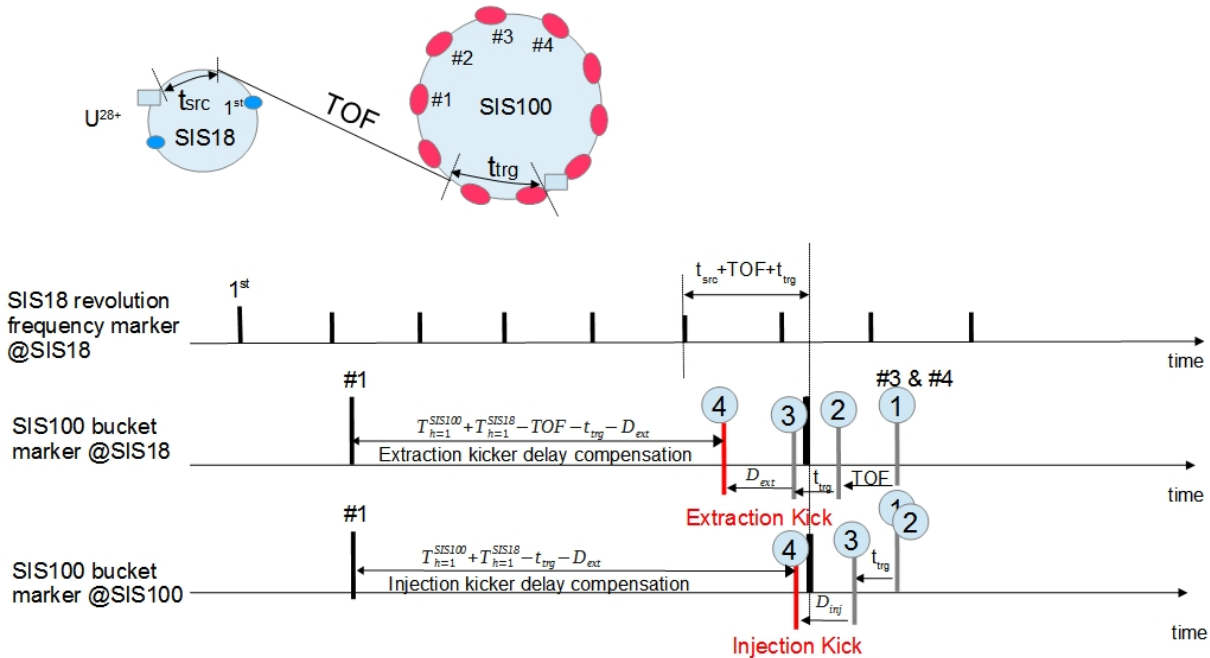


Abbildung 2.1: Synchronization of the SIS18 extraction and SIS100 injection kicker

2.1.5 Beam indication for the beam instrumentation

In order to observe the particle beams and measure related parameters for accelerators and transfer lines, the beam instrumentation equipments must be synchronized and triggered within the beam schedule. For the B2B transfer, the data acquisition for the beam instrumentation equipments should be triggered before the bunch is extracted. But they should not be triggered too early because of the limitation of sampling time. So a pre-trigger is necessary, which indicates that the bunch will be extracted soon, much shorter than the sampling time limitation. For the beam instrumentation system at FAIR, the data acquisition is at a sampling rate of 1GS/s and the upper bound sampling time is 100us.

The beginning of the synchronization window is used for the pre-trigger.

2.2 Prerequisites/boundary conditions for the B2B transfer system

For the FAIR accelerator complex, synchronization of the B2B transfer will be realized by the FAIR control system and the Low-Level RF (LLRF) system. For the synchronization of LLRF system, the GMT system is complemented and linked to the Bunchphase Timing System (BuTiS).

2.2.1 FAIR control system

The FAIR control system takes advantage of collaborations with CERN in using proven framework solutions like FESA, LSA, White Rabbit, etc. It consists of the equipment layer, middle layer and application layer. The equipment layer consists of equipment interfaces, GMT and software representations of the equipment (FESA)Front-End System Architecture. The middle layer provides service functionality both to the equipment layer and the application layer through the IP control system network. LSA is used for the Settings Management. The application layer combines the applications for operators as GUI applications or command line tools. The application layer and the middle layer only request what the FAIR accelerator complex should do and transmit set values to the equipment layer. The actual beam production is controlled by the GMT. The GMT system is synchronized to BuTiS. The SM supplies the schedule for the timing master by LSA.

2.2.1.1 BuTiS

Bunch Phase Timing System (BuTiS) serves as a campus-wide clocks distribution system with subnanosecond resolution and stability over distances of several hundred meters while maintaining 100ps per km timing stability. Two BuTiS reference clocks 10 MHz and 200 MHz and a trigger identification pulse at 100 kHz are generated centrally in the BuTiS center. A star-shaped optical fiber distribution network transfers these signals to BuTiS receivers all over the FAIR campus. A BuTiS receiver and a local reference synthesizer are installed in each supply room to produce the BuTiS reference clocks, which are in phase. For this purpose, a measurement setup in the BuTiS center continuously measures the optical signal transmission delay between the BuTiS center and the different BuTiS receivers. This measurement

information is used to shift the phases of the signals generated in each local reference synthesizer for the delay compensation. The main task of BuTiS is the supply of the reference clock signals for Reference RF Signals in each rf supply rooms.

2.2.1.2 GMT

The GMT is contained in the equipment layer. The main tasks of the GMT system are time synchronization of more than 2000 Front-End Controllers (FEC) with nanosecond accuracy, distribution of timing messages and subsequent generation of real-time actions by the nodes of the timing system. The GMT consists of the Timing Master (TM) and the White Rabbit (WR) timing network and integrates nodes. The timing master's interface to the upper layers, e.g. online schedule monitor, is modeled as a FESA device. The timing master is a logical device, containing the data master (DM), the clock master (CM) and the management master (MM). The data master receives a schedule for the operation of the FAIR accelerator complex from the Settings Management and provides the real-time scheduler by broadcasting messages to the WR timing network, which will be received and executed by the corresponding node at the designated time. The clock master is a dedicated White Rabbit switch. It is the topmost switch layer of the WR timing network and provides the grandmaster clock which is distributed to all other nodes in the timing network. The clock master derives its clock and timestamps from the BuTiS clocks. All active components including receiver nodes and switches are registered to the management master. The management master monitors and manages the active components of the GMT system.

2.2.1.3 FESA

The real-time front-end software architecture FESA is a framework used to fully integrate the large amount of front-end equipments into the FAIR accelerator control system. FESA was developed by CERN and has already been implemented into the CERN control system. FESA develops FESA classes, the equipment-type specific front-end software. For a specific type of equipments, a FESA class implementation accesses to the control interface of the equipments. The FESA class models the equipment as device, so the FESA output is called device class. One device class can instantiate several devices and thus generally handles several independent pieces of equipments. FESA provides JAVA based graphical user interfaces (GUI) to design, deploy, instantiate and test the device classes. The FEC use FESA to implement generic and equipment specific functions in form of the device classes. Interaction with the equipment is synchronized with the GMT system.

FESA (Frontend Software Architecture) [5] is a framework developed at CERN and is now developed further in collaboration with GSI for the FAIR project. It is a toolbox to model abstract device objects where equipment's process variables (sensors and actuators) are represented as properties. The specific equipment access is implemented in C++ by the developer and is linked by the toolchain to the device model to build a so called FESA class (Fig. 4). Then, one or more FESA classes are linked to the run-time core to build an x86-Linux executable. The FESA classes provide a uniform interface via the objectproperty model and a common middle-ware to the upper layers. The device properties are set and read using synchronous or asynchronous access methods (subscription). For time multiplexed operation of the

accelerators, the FESA framework supports defining multiplexed properties. Before an accelerator schedule is started the setting properties of FESA classes are pre-supplied by LSA [6] for all scheduled beams with specific settings accordingly. At runtime, FESA's real time software actions are triggered by timing events, the actual beam specific data is then selected based on information carried by the timing event message and send to the equipment. For the FAIR project the necessary interaction with the timing receiver is realized in a lab-specific timing library of the FESA framework.

2.2.1.4 SM

The SM is located in the middle layer of the control system. It supports off-line generation of machine settings, sending these settings to all involved devices, and programming the schedule of the timing system. The SM uses the LSA (LHC Software Architecture) framework, which originates at CERN and is now developed further in collaboration with GSI for the FAIR project. The settings management is based on a physics model for accelerator optics, parameter space and overall relations between parameters and between accelerators. A standardized API allows accessing data in a common way as basis for generic client applications for all accelerators. Using the LSA-API, trim-applications can coherently modify machine settings. E.g. the service generates timing constraints (e.g. ramp curve) as well as the equipment's data settings (e.g. field) for all devices derived from physics parameters (e.g. beam energy). For FAIR the framework is extended to model the overall schedule of all accelerators. Beams are described as Beam Production Chains to allow a description from beam-source to beamtarget for settings organization and data correlation.

2.2.2 LLRF system

The FAIR low-level rf (LLRF) system shall be usable in the existing machines SIS18 and experimental storage ring (ESR) as well as in the FAIR synchrotrons SIS100 and SIS300 and in the storage rings collector ring (CR), new experimental storage ring (NESR), and accumulator ring (RESR). It supports fast ramp rates and large frequency span for the acceleration of a variety of ion species. It supports different RF manipulations, including operation at different harmonic numbers, barrier bucket generation and bunch compression.

Cavities are driven from a supply room by a Reference RF Signal. Fig. 2.2 shows the typical cavity system with a Reference RF Signal. The cavity gets the RF signal from a local Cavity DDS (Direct Digital Synthesizer) unit, which receives RF Frequency Ramps from the Central Control System (CCS). A DSP-System (Digital Signal Processor) measures the phase between the Reference RF Signal and the gap voltage of the cavity. In the DSP system, a closed-loop control algorithm is implemented which generates frequency corrections for the local Cavity DDS. In this way, it is ensured that the phase of the gap voltage follows the phase of the reference RF signal. The Reference RF Signal distribution shown in Fig. 2.3 is located in each supply room. The Reference RF Signals in different supply rooms are synchronized by the BuTiS. BuTiS 200MHz and 100kHz clock signals are received by BuTiS receivers in different supply rooms in phase. In Fig. 2.3, a number of Group DDS units are located in each supply room, which are synchronized to BuTiS local reference. The Group DDS signals can be routed to the different cavity systems by a Switch

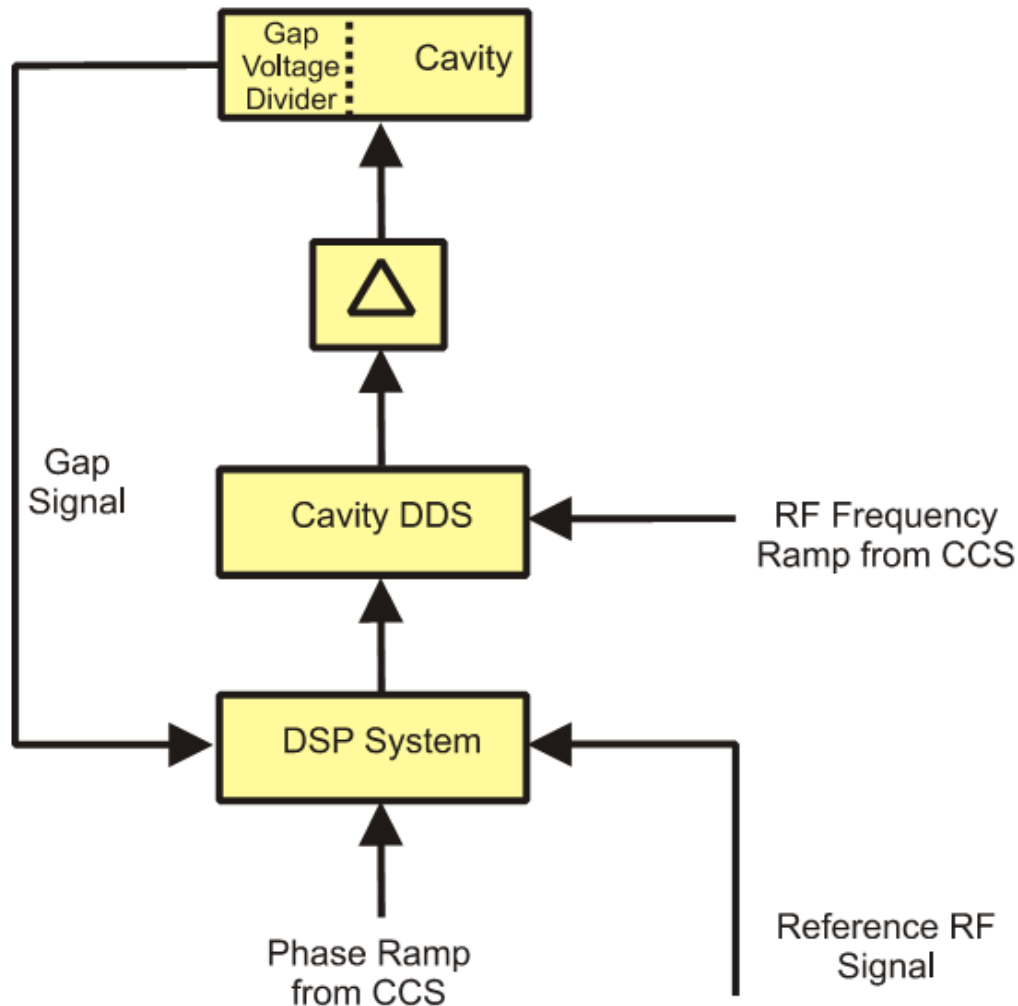


Abbildung 2.2: Local Cavity Synchronization

Matrix. All cavities in a synchrotron could be providing with the same Group DDS signal. The cavities at different harmonic numbers could be realized by using Group DDS signals with different harmonic numbers. The Group DDS concept allows to synchronize a variety of cavities in a very flexible way.

All the cavities of SIS18 are driven from one supply room. The SIS100 cavities will be gathered in three acceleration sections, each of them is driven by a dedicated supply room.

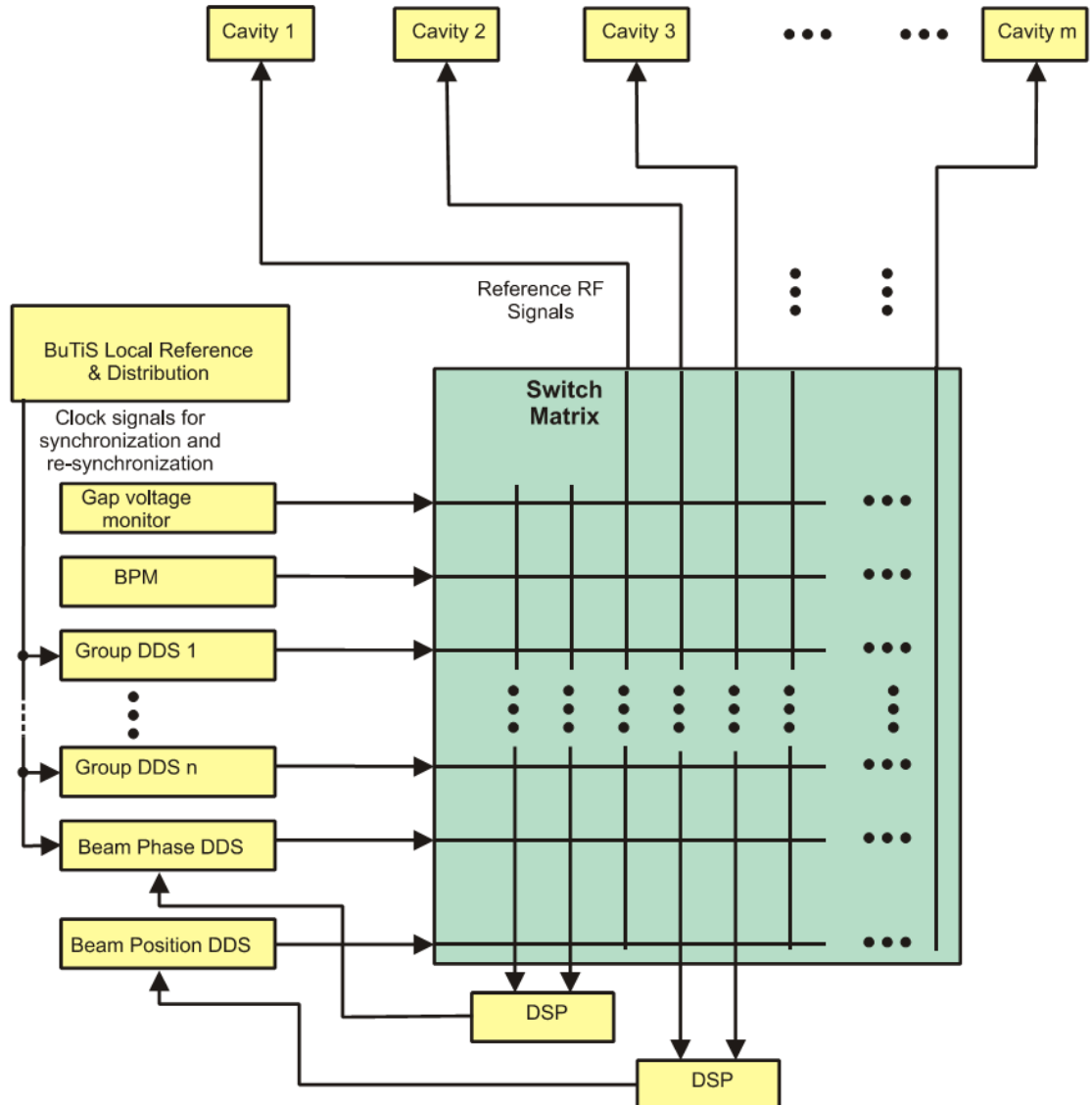


Abbildung 2.3: Reference RF Signal Distribution

Kapitel 3

First idea on the B2B transfer system

3.1 Data acquisition from two synchrotrons

3.2 Coarse synchronization

3.3 Fine synchronization

Kapitel 4

Concept of the B2B transfer system

4.1 Basic procedure of the B2B transfer system for FAIR

Fig. 4.1 illustrates two different possible scenarios for the B2B transfer. The top part shows the chronological steps of the frequency beating method, while the bottom part shows the steps of the phase shift method. The synchronization window must take into account the kicker delay in cables and electronics, as well as the kicker preparation time. The trigger signal must consider the kicker delay compensation. The emergency kickers can be triggered at any time during the acceleration cycle by the MPS3. The yellow region shows the synchronization window. The purple region shows the valid time for the emergency kicker. The B2B transfer process basically needs to follow six steps:

1. The DM announces the B2B transfer and freezes the beam-phase loop, when required.
2. The two synchrotrons measure the rf phase locally.
3. The source synchrotron gathers the measured rf phase from the target synchrotron.
4. The source synchrotron calculates the synchronization window with the kicker delay and sends it to both synchrotrons and to the DM. Besides, it reproduces the bucket label signal at the source synchrotron. For the phase shift method, the source synchrotron generally achieves the phase shift. But when the target synchrotron is empty, the phase shift is achieved at the target synchrotron.
5. Trigger signal is generated for the kickers with the delay compensation.
6. Kicker electronics fire the kickers.

Fig. 4.2 shows the topology of the B2B transfer system.

4.2 Functional blocks and responsibilities

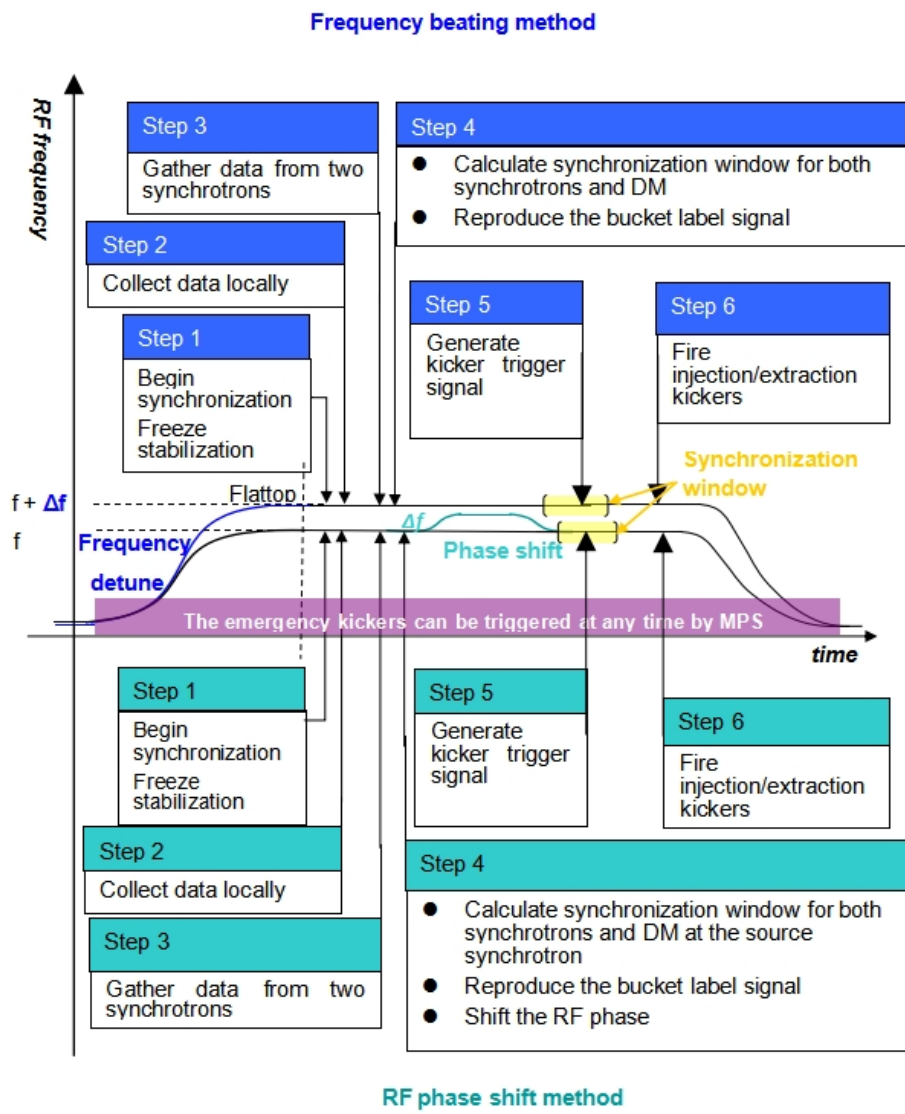


Abbildung 4.1: The procedure for the B2B transfer within one acceleration cycle

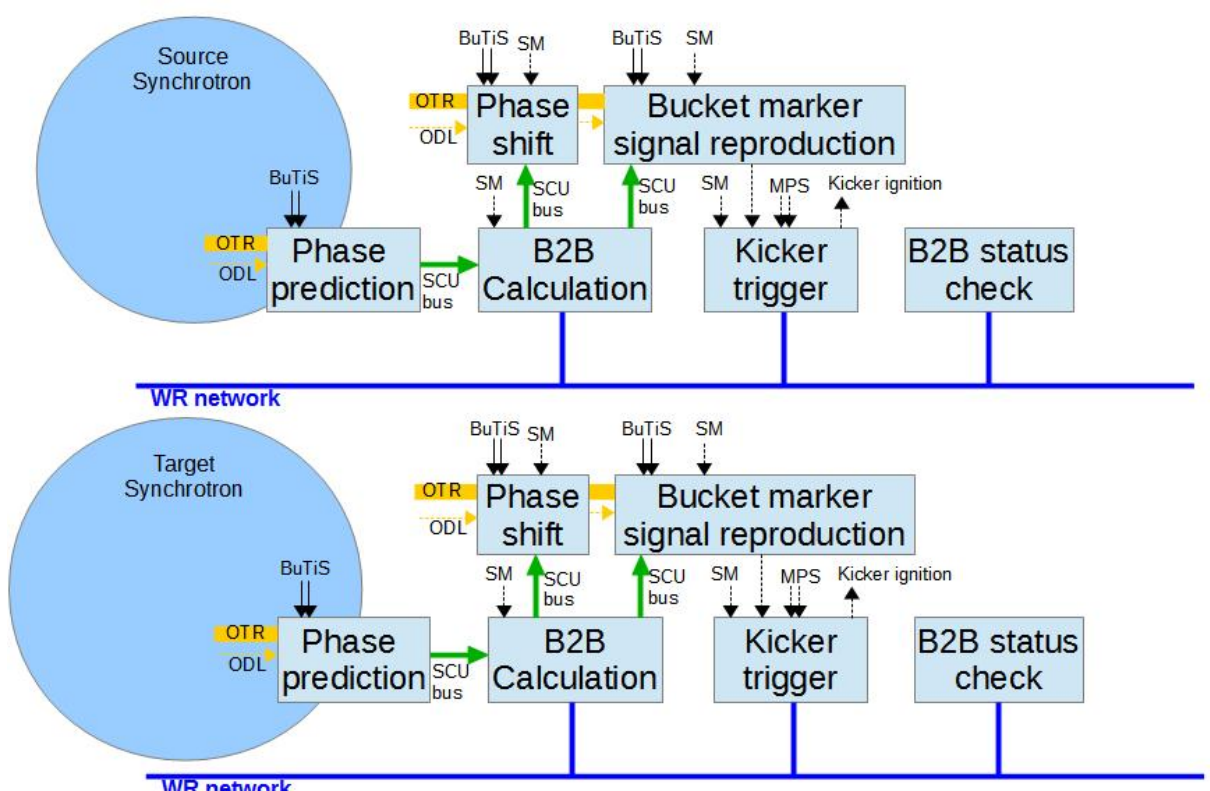


Abbildung 4.2: The topology of the B2B transfer system

Kapitel 5

Realization and systematic investigation of the B2B transfer system

5.1 Investigation from the beam dynamics view for two synchronization methods of U^{28+} for SIS18

This section analyzes the phase shift and frequency beating methods from the beam-dynamics viewpoint for the synchronization of SIS18 with SIS100. In this chapter, the revolution frequency of SIS18 and SIS100 are denoted by $f_{h=1}^{SIS18}$ and $f_{h=1}^{SIS100}$ and the RF frequency by $f_{h=2}^{SIS18}$ and $f_{h=10}^{SIS100}$. Since SIS18 and SIS100 harmonic number is 2 and 10, the relationship between these frequencies is $f_{h=2}^{SIS18} = 2f_{h=1}^{SIS18}$ and $f_{h=10}^{SIS100} = 10f_{h=1}^{SIS100}$.

To achieve a required phase shift, the RF frequency is modulated away from the norminal value. Let $\Delta\phi_{shift}$ be the phase shift to be achieved and $\Delta f(t)$ the RF frequency variation to accomplish it; then,

$$\Delta\phi_{shift} = 2\pi \int_{t_0}^{t_0+T} \Delta f(t) dt \quad (5.1)$$

where T is the period of frequency modulation and t_0 is the time at which the modulation begins. To make the frequency modulation effective, the stabilization system must be frozen before the modulation begins.

I consider here the following four examples of frequency modulation; Case (1) rectangle modulation, Case (2) triangular modulation, Case (3) biased sinusoidal modulation and Case (4) parabola modulation. In order to gaurantee the adiabaticity of these manipulations, I make use the maximum time derivative of rf frequency during the acceleration ramp as the reference, $df/dt=64\text{Hz}/\text{ms}$. Here we assume the phase shift must be achieved within 7ms. These frequency modulations are shown in Fig. 5.1. All the four modulations give the same phase shift, $\Delta\phi_{shift} = \pi$, which is proved by substituting each form of $\Delta f(t)$ into eq. 5.1 and performing integration. Fig. 5.2 shows the time derivation of four rf frequency modulatons.

Case (1)

$$\Delta f_{rf}(t) = \begin{cases} 50\text{Hz}/ms \times (t - t_0) & t_0 + 0 < t \leq t_0 + 2\text{ms} \\ 100\text{Hz} & t_0 + 2 < t \leq t_0 + 5\text{ms} \\ 100\text{Hz} - 50\text{Hz}/ms \times (t - t_0) & t_0 + 5\text{ms} < t \leq t_0 + 7\text{ms} \end{cases} \quad (5.2)$$

Case (2)

$$\Delta f_{rf}(t) = \begin{cases} \frac{10^3}{7 \times 3.5} \text{Hz}/ms \times (t - t_0) & t_0 + 0 < t \leq t_0 + 3.5\text{ms} \\ \frac{10^3}{7} \text{Hz} - \frac{10^3}{7 \times 3.5} \text{Hz}/ms \times (t - t_0 - 3.5\text{ms}) & t_0 + 3.5\text{ms} < t \leq t_0 + 7\text{ms} \end{cases} \quad (5.3)$$

Case (3)

$$\Delta f_{rf}(t) = \frac{10^3}{14} \text{Hz} \times (1 - \cos(\frac{2\pi}{7} \text{rad}/\text{ms} \times (t - t_0))) \quad t_0 + 0 < t \leq t_0 + 7\text{ms} \quad (5.4)$$

Case (4)

$$\Delta f_{rf}(t) = \begin{cases} 30\text{Hz}/ms^2 \times (t - t_0)^2 & t_0 + 0 < t \leq t_0 + 1\text{ms} \\ 30\text{Hz} + 60\text{Hz}/ms \times (t - t_0 - 1\text{ms}) & t_0 + 1\text{ms} < t \leq t_0 + 2.5\text{ms} \\ 30\text{Hz}/ms^2 \times [5\text{ms} - (t - t_0 - 3.5\text{ms})^2] & t_0 + 2.5\text{ms} < t \leq t_0 + 4.5\text{ms} \\ 30\text{Hz} + 60\text{Hz}/ms \times (6\text{ms} - t - t_0) & t_0 + 4.5\text{ms} < t \leq t_0 + 6\text{ms} \\ 30\text{Hz}/ms^2 \times [7\text{ms} - (t - t_0)]^2 & t_0 + 6\text{ms} < t \leq t_0 + 7\text{ms} \end{cases} \quad (5.5)$$

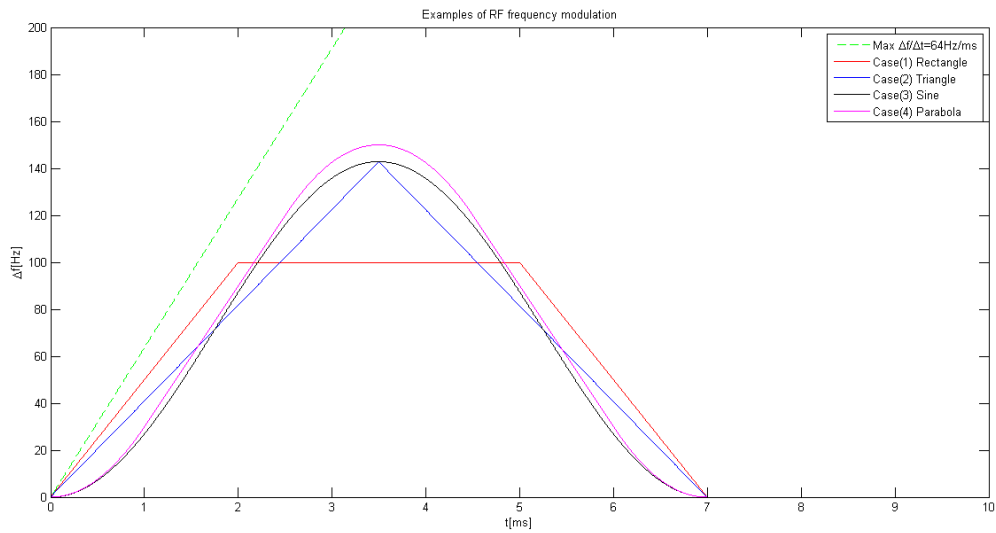


Abbildung 5.1: Examples of RF frequency modulation.

5.1.1 Longitudinal dynamic analysis for the simulation

- Average radial excursion and the relative momentum shift

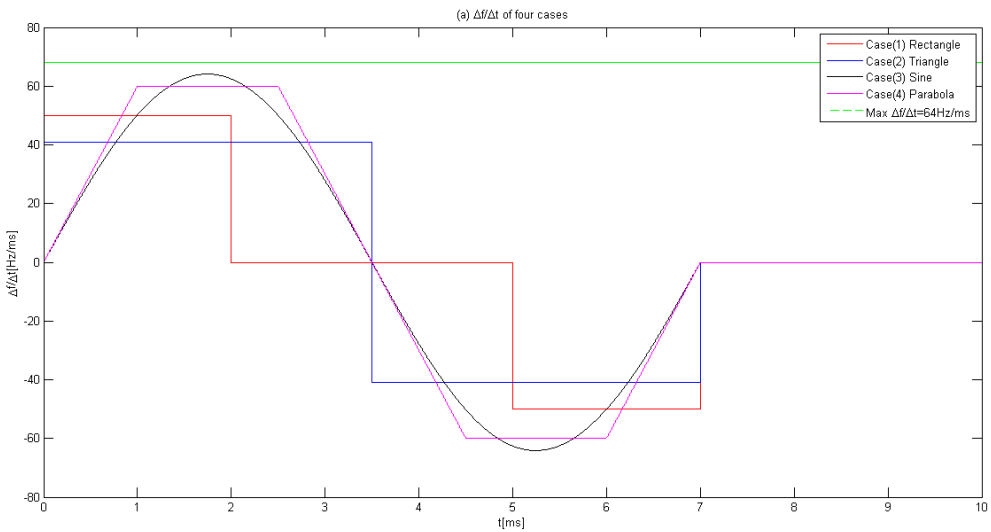


Abbildung 5.2: Time derivation of four modulations

The average radial excursion and the relative momentum shift are calculated for the four kinds of RF frequency modulations by eq. (2.17) and eq. (2.18), see Fig. 5.3 and Fig. 5.4. The momentum modulation and radial excursion of four cases are much smaller than the maximum momentum modulation ± 0.008 and maximum radial excursion $\pm 2.4 \times 10^{-4}$ of SIS18. From the view point of the average radial excursion and the relative momentum shift, four cases of RF frequency modulations are available.

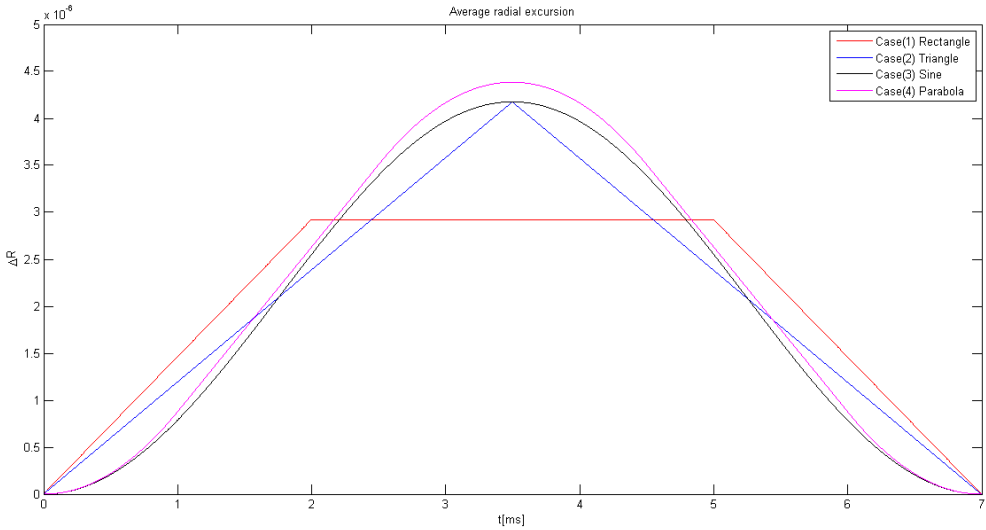


Abbildung 5.3: Average radial excursions for four cases.

- Synchronous phase

The RF frequency modulations make the synchronous phase deviate from the nominal value 0° . Fig. 5.5 shows the changes in synchronous phase, $\Delta\phi_s(t)$, caused by RF frequency modulations for four cases, calculated by introducing

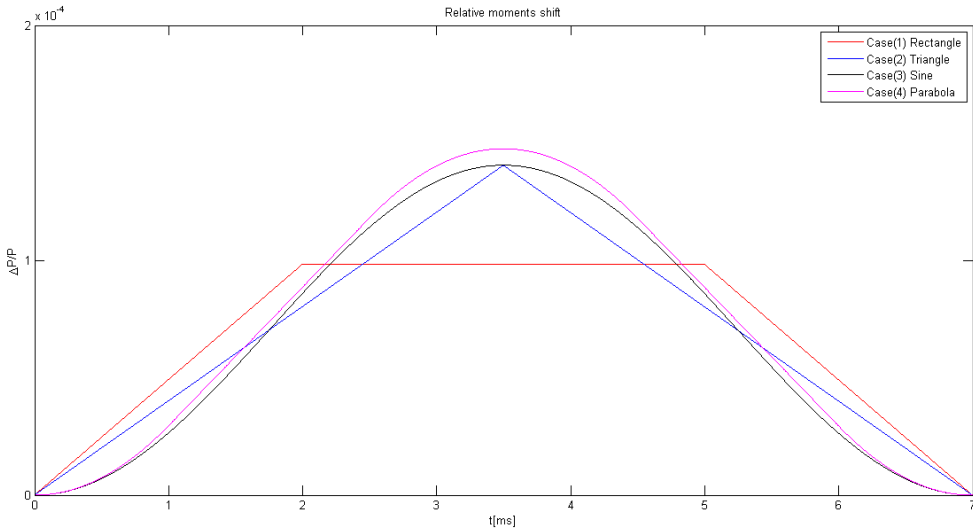


Abbildung 5.4: Relative momentum shifts for four cases.

values into eq. (??). For case (1), jumps in $\Delta\phi_s(t)$ appear at the start and end of the frequency modulation, and at two points where the slope of modulation changes from upward to flat and from flat to downward. For case (2), jumps in $\Delta\phi_s(t)$ appear at the start and end of the frequency modulation, and at the midpoint where the slope of modulation changes from upward to downward. The jumps in $\Delta\phi_s(t)$ are dangerous for beam to follow. For case (3) and (4), the synchronous phase $\Delta\phi_s(t)$ during the modulations are continuous.

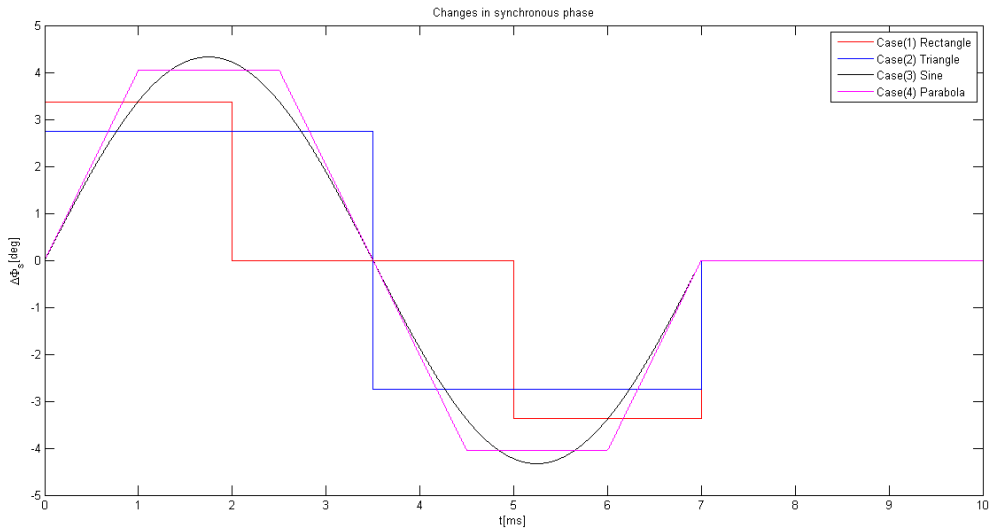


Abbildung 5.5: Changes in synchronous phase caused by RF frequency modulations for four cases

- Bucket size

The bucket area factor $\alpha_b(\phi_s)$ varies during rf frequency modulations. Before the modulations, the synchronous phase $\phi_s = 0^\circ$ and $\alpha_b(0^\circ) = 1$. By intro-

ducing the changes in synchronous phase into eq. (5.6), we get the ratio of bucket areas for four cases, see Fig. (5.6). Four rf frequency modulations have the bucket area factor better than 85%.

$$\alpha_b(\phi_s) \approx (1 - \sin\phi_s)(1 - \sin\phi_s) \quad (5.6)$$

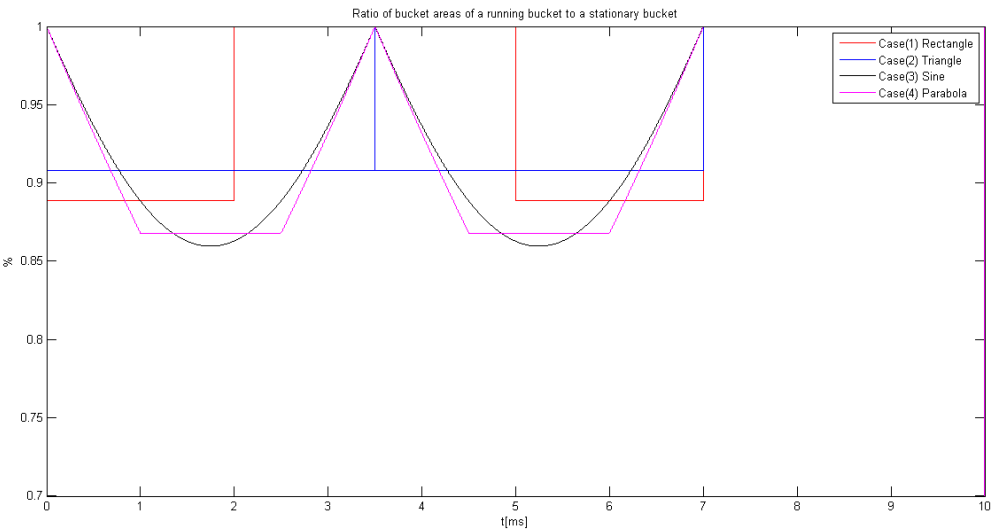


Abbildung 5.6: Ratio of bucket areas of a running bucket to the stationary bucket for four cases

- Adiabaticity

By substituting the values of $d\Delta\phi_s(t)/dt$ obtained from Fig. 5.5 and the other appropriate values into eq. ??, we can calculate the adiabaticity parameter, ε , for the case (3) and (4), see Fig. 5.7. For the case (1) and (2), however, we cannot calculate $d\psi_s(t)/dt$ directly from $\psi_s(t)$ shown in Fig. 5.5, because $\psi_s(t)$ changes discontinuously.

For case (4), the maximum of ε , 0.000059, occurs at 1ms, 2.5ms, 4.5ms and 6ms. From Fig. 5.5, we could see the change of the synchronous phase $d\Delta\phi_s(t)/dt$ is big but smoothly at these time points. For case (3), the maximum of ε is 0.000030.

5.1.2 Transverse dynamics analysis for the simulations

From Fig. 5.4, we could get the maximum momentum shift for four cases. The maximum value of $\Delta p/p$ is around 4.17×10^{-6} at 3.5ms for Cases (2) and (3), around 4.38×10^{-6} at 7.5ms for Case (4) and around 2.92×10^{-6} from 2ms to 5ms for Case (1). For SIS18, the chromaticity Q_x and Q_y is 4.17 and 3.4. Substituting chromaticity and maximum momentum shift into eq. 2.19. We could get the chromatic tune shift during rf modulations for four cases.

Case (1)

$$\Delta Q_x = 4.17 \times 2.92 \times 10^{-6} = 1.22 \times 10^{-5} \quad (5.7)$$

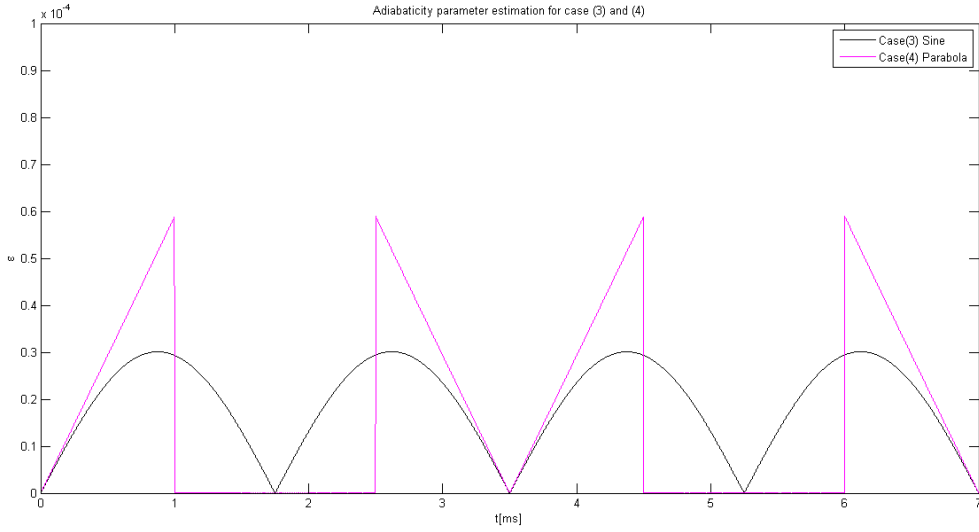


Abbildung 5.7: Adiabaticity parameter estimation for case (3) and (4)

$$\Delta Q_y = 3.4 \times 2.92 \times 10^{-6} = 9.92 \times 10^{-6} \quad (5.8)$$

Case (2) and (3)

$$\Delta Q_x = 4.17 \times 4.17 \times 10^{-6} = 1.74 \times 10^{-5} \quad (5.9)$$

$$\Delta Q_y = 3.4 \times 4.17 \times 10^{-6} = 1.42 \times 10^{-5} \quad (5.10)$$

Case (4)

$$\Delta Q_x = 4.17 \times 4.38 \times 10^{-6} = 1.83 \times 10^{-5} \quad (5.11)$$

$$\Delta Q_y = 3.4 \times 4.38 \times 10^{-6} = 1.49 \times 10^{-5} \quad (5.12)$$

The chromatic tune shift for four cases are significantly small.

5.1.3 Longitudinal dynamics analysis of the frequency beating for SIS18

For the frequency beating method, the RF frequency detuning at the U^{28} 200MeV/ μ extraction energy is 200Hz. Then $\Delta f/f$ is 1.27×10^{-4} . Substituting $\Delta f/f$ into eq. 2.38 and eq. 2.39, we could get the radial excursion and the magnetic field change.

$$\frac{\Delta R}{R} = -\frac{\Delta f}{f} = -1.27 \times 10^{-4} \quad (5.13)$$

$$\frac{\Delta B}{B} = \frac{\Delta f}{f} \gamma_t^2 = 1.27 \times 10^{-4} \times 5.8^2 = 4.27 \times 10^{-3} \quad (5.14)$$

5.2 GMT systematic investigation for the B2B transfer system

5.2.1 Calculation of the synchronization window and its uncertainty

Principally speaking, the synchronization window is a time frame within which the bunch could be injected into the bucket with the bunch to bucket center mismatch better than 1° . In fact, we need just two SIS100 revolution periods long, achieving much preciser injection. The ideal beginning of the synchronization window denotes by WIN_{start} . The synchronization window is within the range $[WIN_{start}, WIN_{start} + 2 \times T_{rev}^{SIS100}]$. T_{rev}^{SIS100} is the revolution period of SIS100, which equals to 6.359 us for U²⁸⁺ at 200Mev/u. The uncertainties in the phase prediction and rf cavity frequency cause an uncertainty δWIN_{start} to the WIN_{start} . The rf cavity harmonic of SIS18 is 2 and that of SIS100 is 10. The Phase advance prediction module extrapolates the rf phase $\psi_{h=1}^{SIS100}$ for SIS100 rf h=1 signal and $\psi_{h=1/5}^{SIS18}$ for SIS18 rf h=1/5 signal at t_ψ . The phase prediction needs 500us. More details about the phase advance measurement and phase advance prediction modules, please see Tibo's thesis. Fig. 5.8 illustrates some basic definition of symbols for the calculation. $\phi_{h=2}^{SIS18}$ and $\phi_{h=10}^{SIS100}$ are individual

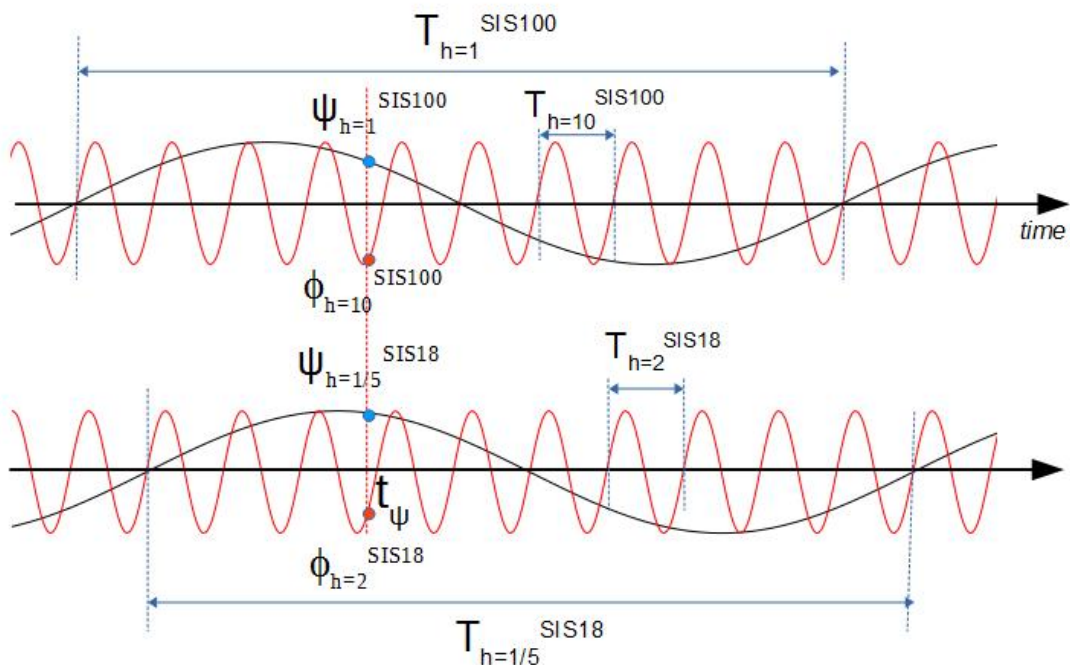


Abbildung 5.8: The illustration of symbols for SIS100

rf phase of SIS18 and SIS100 rf reference signals at t_ψ . The relationship between $\phi_{h=2}^{SIS18}$, $\phi_{h=10}^{SIS100}$ and $\psi_{h=1/5}^{SIS18}$, $\psi_{h=1}^{SIS100}$ are given by eq. 5.18 and eq. 5.17. The uncertainty

of $\psi_{h=1/5}^{SIS18}$ and $\psi_{h=1}^{SIS100}$ is 0.05° .

$$\phi_{h=2}^{SIS18} = \frac{\frac{\psi_{h=1/5}^{SIS18}}{360^\circ} \times T_{h=1/5}^{SIS18} \bmod T_{h=2}^{SIS18}}{T_{h=2}^{SIS18}} \times 360^\circ \quad (5.15)$$

$$\phi_{h=10}^{SIS100} = \frac{\frac{\psi_{h=1}^{SIS100}}{360^\circ} \times T_{h=1}^{SIS100} \bmod T_{h=10}^{SIS100}}{T_{h=10}^{SIS100}} \times 360^\circ \quad (5.16)$$

substituting $T_{h=2}^{SIS18} \times 10 = T_{h=1/5}^{SIS18}$, $T_{h=10}^{SIS100} \times 10 = T_{h=1}^{SIS100}$ into eq.5.17 and eq.5.18 yields

$$\phi_{h=2}^{SIS18} = \frac{\frac{\psi_{h=1}^{SIS18} \times 10}{360^\circ} \times T_{h=2}^{SIS18} \bmod T_{h=2}^{SIS18}}{T_{h=2}^{SIS18}} \times 360^\circ \quad (5.17)$$

$$\phi_{h=10}^{SIS100} = \frac{\frac{\psi_{h=1}^{SIS100} \times 10}{360^\circ} \times T_{h=10}^{SIS100} \bmod T_{h=10}^{SIS100}}{T_{h=10}^{SIS100}} \times 360^\circ \quad (5.18)$$

The uncertainty of $\phi_{h=2}^{SIS18}$ and $\phi_{h=10}^{SIS100}$ are

$$\delta\phi_{h=2}^{SIS18} = \sqrt{\left(\frac{\partial\phi_{h=2}^{SIS18}}{\partial\psi_{h=2}^{SIS18}}\delta\psi_{h=2}^{SIS18}\right)^2} = \sqrt{(10 \times \delta\psi_{h=2}^{SIS18})^2} = 0.5^\circ \quad (5.19)$$

$$\delta\phi_{h=10}^{SIS100} = \sqrt{\left(\frac{\partial\phi_{h=10}^{SIS100}}{\partial\psi_{h=10}^{SIS100}}\delta\psi_{h=10}^{SIS100}\right)^2} = \sqrt{(10 \times \delta\psi_{h=10}^{SIS100})^2} = 0.5^\circ \quad (5.20)$$

When we change the uncertainty of $\phi_{h=2}^{SIS18}$ and $\phi_{h=10}^{SIS100}$ at t_ψ from phase to time domain. The uncertainty of t_ψ is

$$\delta t_\psi = \frac{\delta\psi_{h=2}^{SIS18}}{360^\circ} \times \frac{1}{157KHz} = \frac{0.05^\circ}{360^\circ} \times \frac{1}{157KHz} \approx 1ns \quad (5.21)$$

5.2.1.1 Synchronization window for the phase shift method and its uncertainty

Different relation between $\phi_{h=2}^{SIS18}$ and $\phi_{h=10}^{SIS100}$ has different required phase adjustment for SIS18. Fig. 5.9 illustrates all scenarios of their relation and the required phase adjustment for each scenario. The blue and red line represents the phase of SIS100 and SIS18 rf reference signal. The clockwise arrow from the SIS18 to SIS100 rf phase represents the negative phase adjustment for SIS18, and the anticlockwise represents the positive phase adjustment for SIS18. The required phase adjustment of SIS18 is denoted by $\Delta\phi_{shift}$.

- $\phi_{h=10}^{SIS100} \in [0, 90^\circ]$, see Fig. 5.10 (a).
 - $\phi_{h=10}^{SIS100} < \phi_{h=2}^{SIS18} < \phi_{h=10}^{SIS100} + 180^\circ$, which denotes by the yellow semicircle in Fig. 5.10 (a).

$$\Delta\phi_{shift} = -(\phi_{h=2}^{SIS18} - \phi_{h=10}^{SIS100}) \quad (5.22)$$

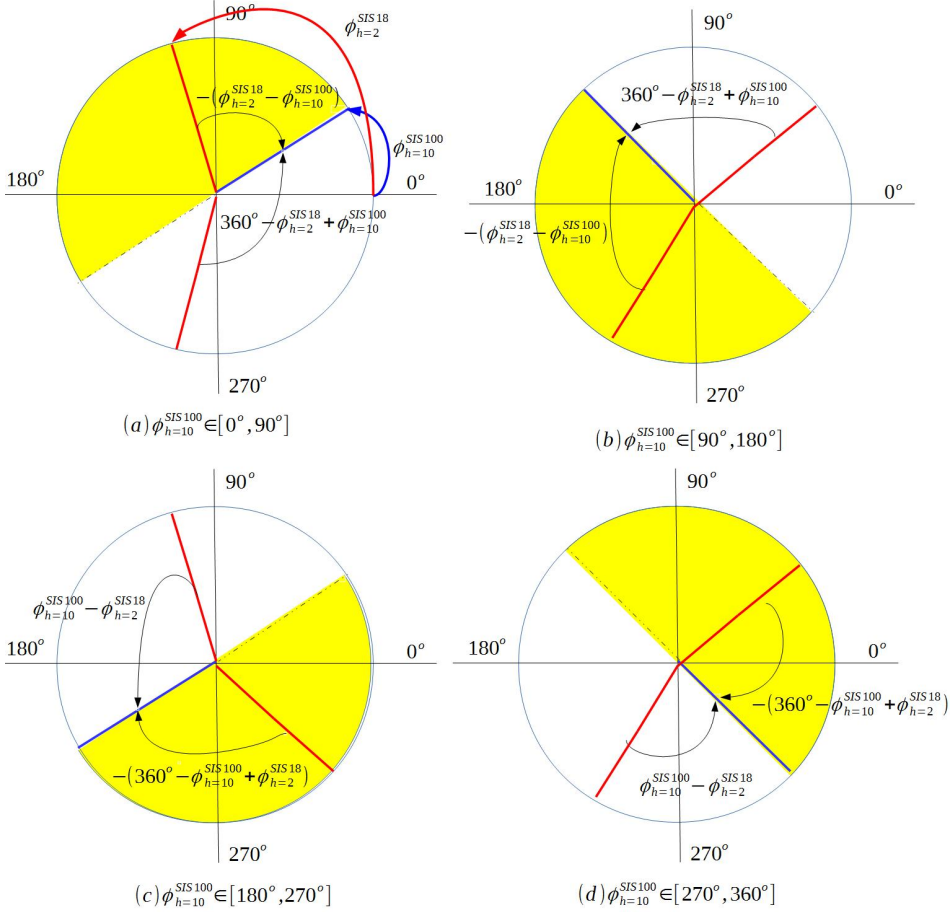


Abbildung 5.9: Scenarios for the phase shift method

- $\phi_{h=2}^{SIS18} < \phi_{h=10}^{SIS100}$ or $\phi_{h=2}^{SIS18} > \phi_{h=10}^{SIS100} + 180^\circ$, which denotes by the white semicircle in Fig. 5.10 (a).

$$\Delta\phi_{shift} = 360^\circ - \phi_{h=2}^{SIS18} + \phi_{h=10}^{SIS100} \quad (5.23)$$

- $\phi_{h=10}^{SIS100} \in [90, 180^\circ]$, see Fig. 5.10 (b).

- $\phi_{h=2}^{SIS18} < \phi_{h=10}^{SIS100}$ or $\phi_{h=2}^{SIS18} > \phi_{h=10}^{SIS100} + 180^\circ$, which denotes by the yellow semicircle in Fig. 5.10 (b).

$$\Delta\phi_{shift} = -(\phi_{h=2}^{SIS18} - \phi_{h=10}^{SIS100}) \quad (5.24)$$

- $\phi_{h=10}^{SIS100} < \phi_{h=2}^{SIS18} < \phi_{h=10}^{SIS100} + 180^\circ$, which denotes by the white semicircle in Fig. 5.10 (b).

$$\Delta\phi_{shift} = 360^\circ - \phi_{h=2}^{SIS18} + \phi_{h=10}^{SIS100} \quad (5.25)$$

- $\phi_{h=10}^{SIS100} \in [180, 270^\circ]$, see Fig. 5.10 (c).

- $\phi_{h=2}^{SIS18} > \phi_{h=10}^{SIS100}$ or $\phi_{h=2}^{SIS18} < \phi_{h=10}^{SIS100} + 180^\circ - 360^\circ$, which denotes by the yellow semicircle in Fig. 5.10 (c).

$$\Delta\phi_{shift} = -(360^\circ - \phi_{h=10}^{SIS100} + \phi_{h=2}^{SIS18}) \quad (5.26)$$

- $\phi_{h=10}^{SIS100} - 180^\circ < \phi_{h=2}^{SIS18} < \phi_{h=10}^{SIS100}$, which denotes by the white semicircle in Fig. 5.10 (c).

$$\Delta\phi_{shift} = \phi_{h=10}^{SIS100} - \phi_{h=2}^{SIS18} \quad (5.27)$$

- $\phi_{h=10}^{SIS100} \in [270, 360^\circ]$, see Fig. 5.10 (d).

- $\phi_{h=10}^{SIS100} - 180^\circ < \phi_{h=2}^{SIS18} < \phi_{h=10}^{SIS100}$, which denotes by the yellow semicircle in Fig. 5.10 (d).

$$\Delta\phi_{shift} = -(360^\circ - \phi_{h=10}^{SIS100} + \phi_{h=2}^{SIS18}) \quad (5.28)$$

- $\phi_{h=2}^{SIS18} > \phi_{h=10}^{SIS100}$ or $\phi_{h=2}^{SIS18} < \phi_{h=10}^{SIS100} + 180^\circ - 360^\circ$, which denotes by the white semicircle in Fig. 5.10 (d).

$$\Delta\phi_{shift} = \phi_{h=10}^{SIS100} - \phi_{h=2}^{SIS18} \quad (5.29)$$

The phase adjustment is achieved by the phase shfit method within the upper bound time, $T_{phaseshift}^{upperbound}$. For the U^{28} B2B transfer from SIS18 to SIS100, $T_{phaseshift}^{upperbound}$ equals to 7ms. The phase shift $\Delta\phi_{shift}$ is achieved within 7ms. The beginning of the synchronization window is expressed by

$$WIN_{start} = t_\psi - 500\mu s + T_{phaseshift}^{upperbound} \quad (5.30)$$

The uncertainty in the phase prediction $\psi_{h=1/5}^{SIS18}$ and $\psi_{h=1}^{SIS100}$ equals to the uncertainty of t_ψ , $\delta t_\psi = 1\text{ns}$. The phase shift uncertainty $\delta\Delta\phi_{phase}$ equals to the uncertainty in the phase shift upper bound time, $\delta T_{phaseshift}^{upperbound} = 100\text{ps}$. Both causes an uncertainty in the WIN_{start} .

$$\begin{aligned} \delta WIN_{start} &= \sqrt{\left(\frac{\partial WIN_{start}}{\partial t_\psi} \delta t_\psi\right)^2 + \left(\frac{\partial WIN_{start}}{\partial T_{phaseshift}^{upperbound}} \delta T_{phaseshift}^{upperbound}\right)^2} \\ &= \sqrt{(\delta t_\psi)^2 + (T_{phaseshift}^{upperbound})^2} = \sqrt{1\text{ns}^2 + 100\text{ps}^2} = 1\text{ns} \end{aligned} \quad (5.31)$$

The synchronization window uncertainty of the phase shift method could be negligible. So the synchronization window is $[WIN_{start}, WIN_{start} + 2 * 6.359\mu s]$ for U^{28+} B2B transfer from SIS18 to SIS100.

5.2.1.2 Synchronization window for the frequency beating method and its uncertainty

Fig. 5.10 illustrates two scenarios for the frequency beating method. The frequency beating method can only achieve positive phase adjustment, which is denoted by $\Delta\phi_{adjustment}$. Δt is the beating time.

$$\Delta t = \frac{\Delta\phi_{adjustment}}{360^\circ \times \Delta f} \quad (5.32)$$

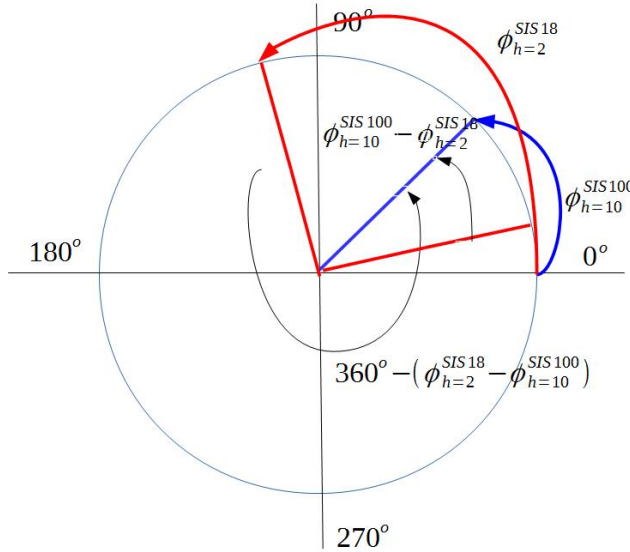


Abbildung 5.10: Two scenarios for the frequency beating method

- $\phi_{h=2}^{SIS18} \geq \phi_{h=10}^{SIS100}$

$$\Delta\phi_{adjustment} = \phi_{h=10}^{SIS100} - \phi_{h=2}^{SIS18} \quad (5.33)$$

Replacing $\Delta\phi_{adjustment}$ in eq. 5.37 with eq. 5.33, we have

$$\Delta t = \frac{\phi_{h=10}^{SIS100} - \phi_{h=2}^{SIS18}}{360^\circ \times \Delta f} \quad (5.34)$$

$$WIN_{start} = t_\psi - 500\text{us} + \Delta t = t_\psi - 500\text{us} + \frac{\phi_{h=10}^{SIS100} - \phi_{h=2}^{SIS18}}{360^\circ \times \Delta f} \quad (5.35)$$

- $\phi_{h=2}^{SIS18} < \phi_{h=10}^{SIS100}$

$$\Delta\phi_{adjustment} = 360^\circ - (\phi_{h=2}^{SIS18} - \phi_{h=10}^{SIS100}) \quad (5.36)$$

Replacing $\Delta\phi_{adjustment}$ in eq. 5.37 with eq. 5.36, we have

$$\Delta t = \frac{360^\circ - (\phi_{h=2}^{SIS18} - \phi_{h=10}^{SIS100})}{360^\circ \times \Delta f} \quad (5.37)$$

$$WIN_{start} = t_\psi - 500\text{us} + \Delta t = t_\psi - 500\text{us} + \frac{360^\circ - (\phi_{h=2}^{SIS18} - \phi_{h=10}^{SIS100})}{360^\circ \times \Delta f} \quad (5.38)$$

Based on these two scenarios, we could deduce the formulas for the start of the synchronization window.

$$WIN_{start} = t_\psi - 500\text{us} + \Delta t = t_\psi - 500\text{us} + \frac{\Delta n \times 360^\circ - (\phi_{h=2}^{SIS18} - \phi_{h=10}^{SIS100})}{360^\circ \times \Delta f} \quad (5.39)$$

where Δn equals 1 when $\phi_{h=2}^{SIS18} < \phi_{h=10}^{SIS100}$ and equals 0 when $\phi_{h=2}^{SIS18} \geq \phi_{h=10}^{SIS100}$. The uncertainties in the phase prediction and rf frequency detune cause an uncertainty

in the WINstart. $\delta\Delta f$ is $\pm 38\text{Hz}$, 24ppm . $\delta\phi_{h=2}^{SIS18}$ and $\delta\phi_{h=10}^{SIS100}$ are 0.5° . Δf is 200Hz . The maximum $\Delta n \times 2\pi - (\phi_{h=2}^{SIS18} - \phi_{h=10}^{SIS100})$ is 2π .

$$\begin{aligned}
 \delta WIN_{start} &= \sqrt{\left(\frac{\partial WIN_{start}}{\partial \phi_{h=2}^{SIS18}} \delta \phi_{h=2}^{SIS18}\right)^2 + \left(\frac{\partial WIN_{start}}{\partial \phi_{h=10}^{SIS100}} \delta \phi_{h=10}^{SIS100}\right)^2 + \left(\frac{\partial WIN_{start}}{\partial \Delta f} \delta \Delta f\right)^2} \\
 &= \sqrt{\left(\frac{-1}{2\pi \times \Delta f} \delta \phi_{h=2}^{SIS18}\right)^2 + \left(\frac{1}{2\pi \times \Delta f} \delta \phi_{h=10}^{SIS100}\right)^2 + \left(-\frac{\Delta n \times 2\pi - (\phi_{h=2}^{SIS18} - \phi_{h=10}^{SIS100})}{2\pi \times \Delta f^2} \delta \Delta f\right)^2} \\
 &\leq \sqrt{\left(\frac{-1}{2\pi \times 200} 0.5^\circ\right)^2 + \left(\frac{1}{2\pi \times 200} 0.5^\circ\right)^2 + \left(-\frac{2\pi}{2\pi \times 200^2} 38\right)^2} \\
 &\approx 1\text{us}
 \end{aligned} \tag{5.40}$$

So the synchronization window is $[WIN_{start} - 1\text{us}, WIN_{start} - 1\text{us} + 2 * 6.359\text{us}]$.

5.2.2 WR network latency measurement

In this thesis, WR network latency measurement is achieved by the Xena traffic generator, which offers a new class of professional Layer 2-3 Gigabit Ethernet test platform. It performs high-precision performance measurement of throughput, latency, jitter, loss, sequence and mis-ordering errors.

Measurement setup is shown in Fig. 5.11. One Xena traffic generator is used in order to measure frame latency, jitter and packet loss for WR switches. For the measurements, Xena traffic generator sends the traffic streams with a unique stream ID for identifying latency, jitter and packet loss. A Virtual Local Area Network (VLAN) is a group of FECs in the WR network that is logically segmented by function or application, without regard to the physical locations of the FECs. For the WR network for FAIR, four VLANs are applied.

- DM VLAN
 - All FECs in the WR network are assigned to the DM broadcast VLAN, within which the DM forwards broadcast timing telegrams downwards to all FECs. The available average bandwidth for this VLAN corresponds to a rate of 100 Mbit/s . But the traffic is not evenly distributed across all destinations. DM bursts 60 messages at the ahead interval 500us of a message schedule. Burst is a group of consecutive packets with shorter interpacket gaps than packets arriving before or after the burst of packets. The burst speed is 12 packets per 100us .
 - The telegrams sent from the source B2B SCU upwards to the DM are unicast packets within DM unicast VLAN. 2 packets are send within 10 millisecond synchronization period. The maximum repetition frequency is 2.82Hz , the U^{28+} supercycle. So the average bandwidth is 6 packets per second. Besides, DM sends 10Mbps unicast traffic to FECs at the burst speed of 3 packets per 300us .
- B2B VLAN. All SCUs for the B2B transfer are assigned to the B2B VLAN. The specified VLAN for the B2B transfer could reduce the traffic of the WR network. All B2B related broadcast telegrams are broadcasted in this VLAN.

100 packets are send within 10 millisecond synchronization period. The average bandwidth is 28 packets per second

- Low priority VLAN. This VLAN is used for the ... The available average bandwidth for this VLAN corresponds to a rate of 10 Mbps.

In Fig. 5.11, the port connected with the red optical fiber sends packets in the DM VLAN, the port connected with the yellow optical fiber sends packets in the B2B VLAN, and the port connected with the blue optical fiber sends packets in the low priority VLAN. Xena traffic generator sends traffic only directly to the 1st WR switch. Other three WR switches get traffic sequentially from their top layer WR switch. All WR switches send packets back to Xena traffic generator via the black connection, which achieves the latency, jitter and packet loss measurement for each layer switch. The length of all optical fiber in the test is 5 meter, whose latency could be ignored. Because the latency of the optical fiber with 1310 nm wavelength is about $204 \text{ m}/\mu\text{s}$. The latency for 5 meters is about 25ns.

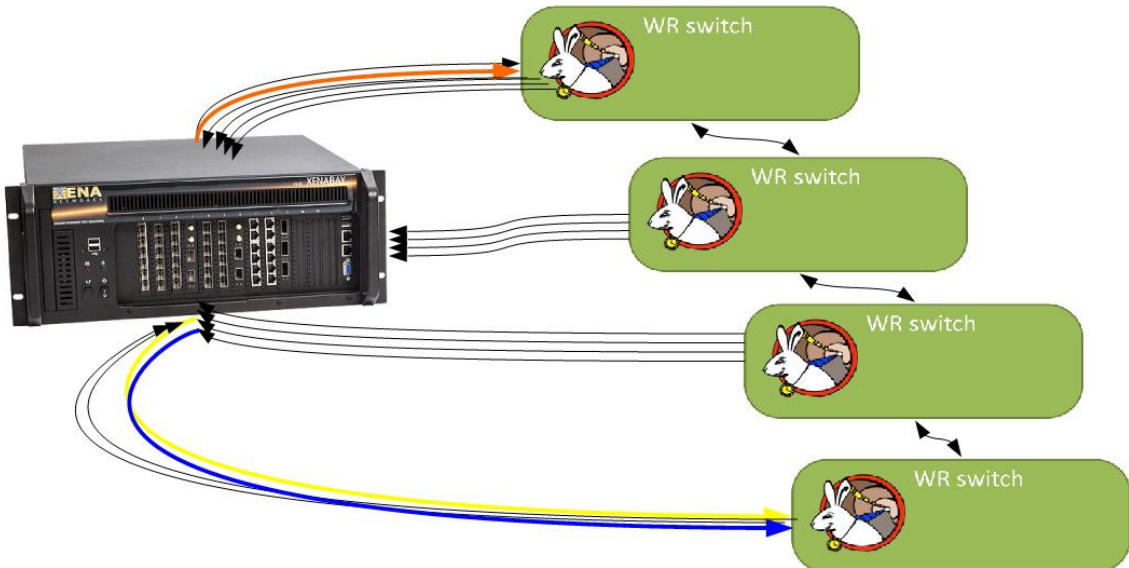


Abbildung 5.11: Schematic of the network setup

Table 5.1 shows the packet latency and jitter measurement result of different layer WR switches. The test lasts for 17 hours and there exists no packet loss.

For the B2B transfer system, the maximum delay for the B2B related packets in the B2B VLAN and DM unicast VLAN is $500\mu\text{s}$. The delay is decided by the number of WR switches and the length of the optical fiber. Even for 2km the delay is only about $10 \mu\text{s}$. So the number of WR switches plays a more important role in the delay. Maximum 10 WR switches are available between the B2B source SCU and B2B target SCU, between B2B source SCU and source trigger SCU and between B2B source SCU and target trigger SCU and maximum 10 WR switches are available between the B2B source SCU and DM.

Tabelle 5.1: The latency of the WR switch

Number of WR switches	DM broadcast VLAN Max delay ± jitter	DM unicast VLAN Max delay ± jitter	B2B VLAN Max delay ± jitter	Low priority Max delay ±
1	16.270us±13.590us	16.126us±13.398us	29.816us±27.109us	33.838us±31
2	17.825us±13.807us	17.825us±13.590us	32.074us±27.157us	38.320us±33
3	20.688us±13.951us	20.616us±13.783us	34.792us±27.133us	40.845us±32
4	23.502us±14.192us	23.358us±13.879us	38.167us±26.722us	44.526us±32

5.3 Kicker systematic investigation for the B2B transfer system

The SIS18 extraction kicker consists of 9 kicker units. In the existing topology, 5 kicker units are installed in the 1st crate and the other 4 units are in the 2nd crate. The width of each kicker unit is 0.25m and the distance between two kicker units is 0.09m. The distance between two crates is 19.167m. SIS100 injection kicker consists of 6 kicker units, which are equally located. The width of each kicker unit is 0.22m and the distance between two units is 0.23m. For the B2B transfer, the rise time of SIS18 extraction kicker and SIS100 injection kicker unit are 90ns and 1/20 of the revolution period. The rise time of these kickers must fit within the bunch gap, 25% of rf reference period. Here we are discussing about the following possibilities.

- For SIS18, whether the kicker units in the 2nd crate could be fired a fixed delay after the firing of the kicker units in the 1st crate for ion beams over the whole range of stable isotopes.
- For SIS100, whether the kicker units could be fired instantaneously.

5.3.1 SIS18 extraction kicker units

Here we take three ion beams, H^+ , U^{28} and U^{73+} , to check the possibility, because the boundary ion species have the most stringent requirements. Fig. 5.12 shows three scenarios of the firing delay between two crates. Beam is firstly kicked by kicker units in the 1st crate and then kicked by the units in the 2nd crate to the transfer line. The yellow and red ellipse represents the position of the bunches, when the kicker units in the 1st and 2nd crate are fired. The number in the ellipse is used to tell different bunches. The head of the bunch is at the right side. The bunch 2 is firstly kicked. Here we assume ...the kicker units in the same crate are triggered instantaneous. The bunch gap is longer than ... d denotes the distance between two crates. L denotes the distance from the leftmost to the rightmost kicker unit. D denotes the sum distance of d and the 2nd crate. d equals to 19.167 meter. L equals to 22.047m = d + 9×0.25m + 7× 0.09m. D equals to 20.437m = d + 4×0.25m + 3× 0.09m.

Figure (a) is the easiest scenario. The kicker units in the 1st crate are fired when the tail of the bunch 1 passes by the 1st crate completely. The kicker units in the

2nd crate are fired when the tail of the bunch 1 passes by the 2nd crate completely. The delay for the firing two crates in this scenario is $D/\beta c$. β is ...

The second plot in Fig. 5.12 shows the scenario of the maximum delay between the firing of two crates. The kicker units in the 1st crate are fired when the tail of the bunch 1 passes by the 1st crate completely. The kicker units in the 2nd crate are fired 90ns before the head of the bunch 2 passes by it. The delay equals to $G+d/\beta c - 90\text{ns}$.

The figure on the bottom shows the scenario of the minimum delay. The kicker units in the 1st crate are fired 90ns before the head of the bunch 2 passes by it. The kicker units in the 2nd crate are fired when the bunch 1 passes by the 2nd crate. The delay is $L/v - G + 90\text{ns}$.

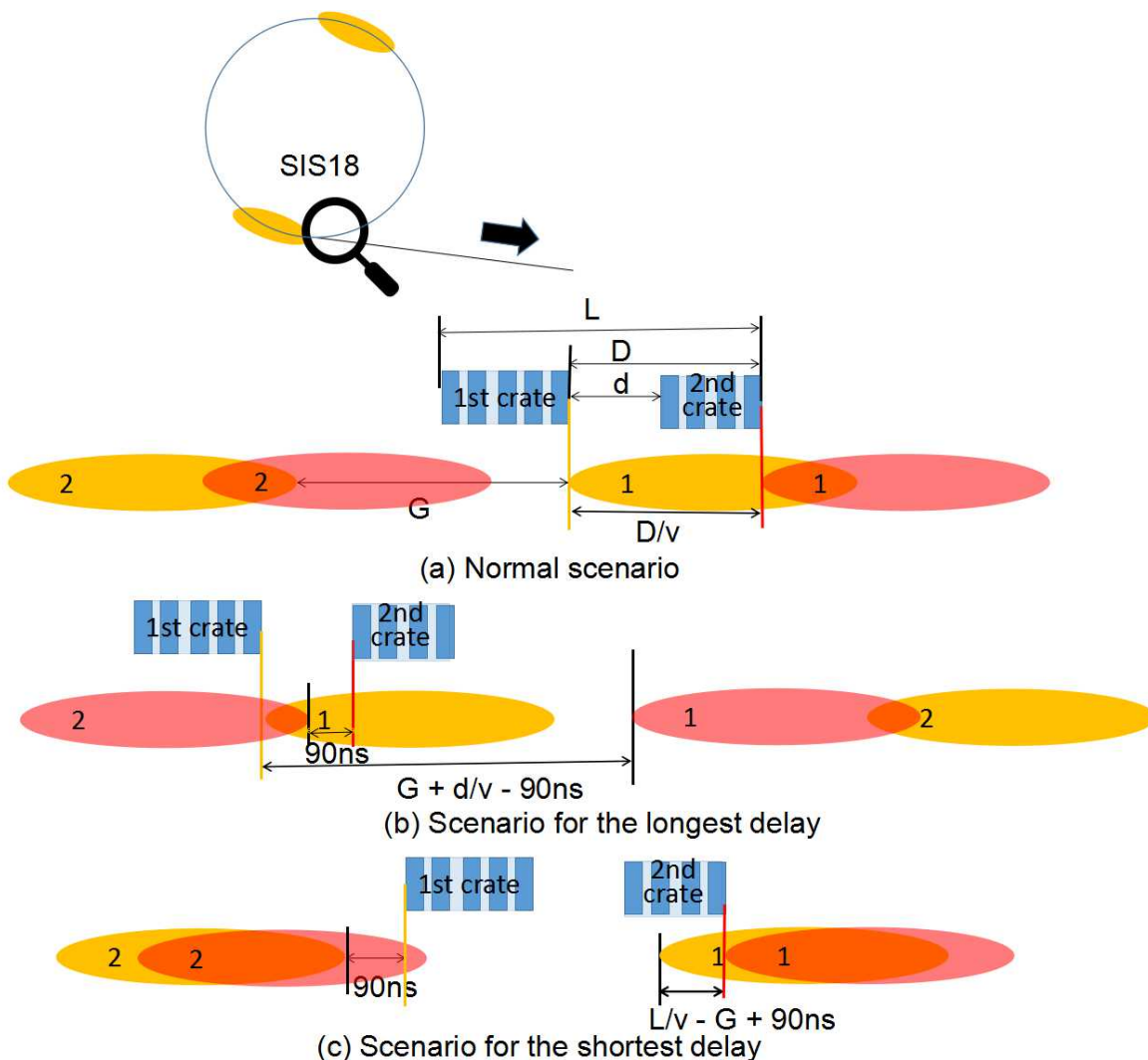


Abbildung 5.12: Three scenarios for the delay of SIS18 extraction kicker

Table 5.2 shows delay for three scenarios and related perimeters. The fixed delay is determined primarily by the boundary delay range from H^+ , U^{28} and U^{73+} beams, the delay range for other heavy ion species beams must be contained in these boundary range. According to the result, a fixed delay is available for firing kicker units in two crate for different beams. e.g. 80ns.

Tabelle 5.2: The delay for firing two crates of SIS18 extraction kicker

Beam	β	time $L/\beta c$	bunch gap G	minimum delay $L/\beta c-G+90\text{ns}$	delay $D/\beta c$	maximum delay $G+d/\beta c-90\text{ns}$
H^+	0.982	75ns	184ns	0ns	69ns	163ns
U^{28}	0.568	130ns	159ns	61ns	120ns	189ns
U^{73+}	0.872	84ns	104ns	70ns	78ns	92ns

5.3.2 SIS100 injection kicker units

Two bunches from SIS18 will be continuously injected into one RF bucket after the other in SIS100. See Fig. 5.3. The yellow ellipse represents the circulating bunch in SIS100 and the red one represents the bunch to be injected. The head of the bunch is at the left side. The preparation of the SIS100 injection kicker must be done during the bunch gap and it must be established for at least one SIS18 revolution period. For the instantaneous firing, all kicker units are fired only if the tail of the circulating bunch passes the leftmost kicker unit. The kicker pass time is the time needed for the tail of a bunch to pass from the rightmost unit to the leftmost kicker unit. The rise time of the kicker unit is 1/20 of the revolution period. Therefor the preparation time is the sum of the kicker pass time and rise time. The distance from the rightmost to the leftmost kicker unit is 3.79m, $6 \times 0.22\text{m} + 5 \times 0.23\text{m}$. If the preparation time is shorter than bunch gap, all kicker units could be fired instantaneous. Table 5.3 shows the preparation time for H^+ , U^{28} and U^{73+} beams and their bunch gap. The preparation time is much shorter than the bunch gap. So the kicker units could be fired instantaneous.

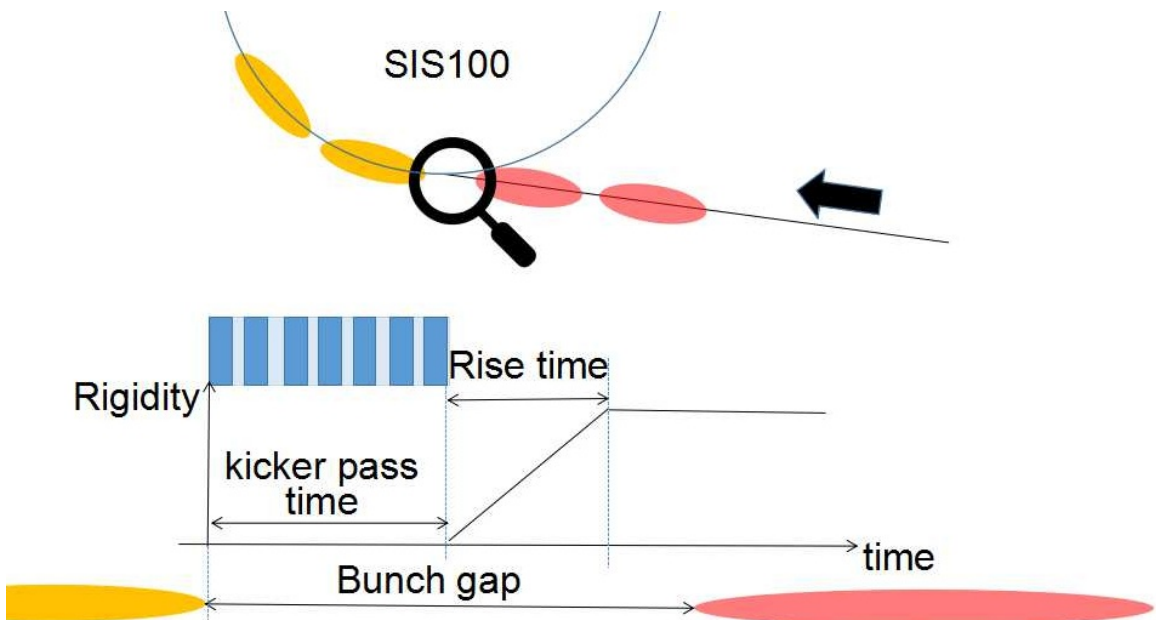


Abbildung 5.13: SIS100 injection kicker

Tabelle 5.3: The delay for firing SIS00 injection kicker

Beam	β	kicker pass time $L/\beta c$	Rise time $1/20 \times T_{rev}^{SIS100}$	Preparasion time $L/\beta c + 1/20 \times T_{rev}^{SIS100}$	bunch gap $2.25 \times T_{rev}^{SIS100}$
H^+	0.982	3ns	184ns	187ns	828ns
U^{28}	0.568	22ns	318ns	333ns	1431ns
U^{73+}	0.872	15ns	207ns	222ns	932ns

5.4 Test setup for the data collection, merging and redistribution of the B2B transfer system

5.4.1 Test requirement

The test setup achieves the following functional requirement.

- After receiving the B2B beginning event, both the B2B source and target SCUs collect predicted phase equivalent data from the source and target synchrotrons locally. The equivalence is a timestamp for the zero crossing point of the simulated RF reference signal.
- The B2B target SCU transfers the telegram containing the timestamp to the B2B source SCU.
- After receving the data, the B2B source SCU calculates the synchronization window.
- The B2B source SCU sends the telegram containing the beginning of the synchronization window to the WR network.
- After receving the telegram, the trigger SCU produces TTL output indicating the synchronization window.

5.4.2 Test setup introduction

Fig. 5.14 shows the schematic of the test setup. In this test setup, I use two MODEL DS345 Synthesized Function Generators with the frequency accuracy of $\pm 5\text{ppm}$ of the selected frequency to simulate RF reference signals of SIS18 and SIS100. DS345 of SIS18 is directly triggered by the 10MHz of BuTiS receiver and DS345 of SIS100 is triggered by DS345 of SIS18. So both DS345s are synchronized to BuTiS. The B2B source SCU, B2B target SCU and trigger SCU are connected to the same WR switch, which connects to the WR network. PC is used to produce timing event and monitor the status of the B2B transfer programs in all SCUs. The oscilloscope is used to monitor the alignment of the two simulated RF reference signals within the synchronization window provided by the trigger SCU.

Fig. 5.15 shows the front and back view of the test setup. DS345 of SIS18 produces the sine wave of 1.572200MHz frequency for the B2B source SCU. DS345 of SIS100 produces the sine wave of 1.1572MHz for the B2B target SCU. So the beating frequency is 200Hz and the synchronization period is 5ms.

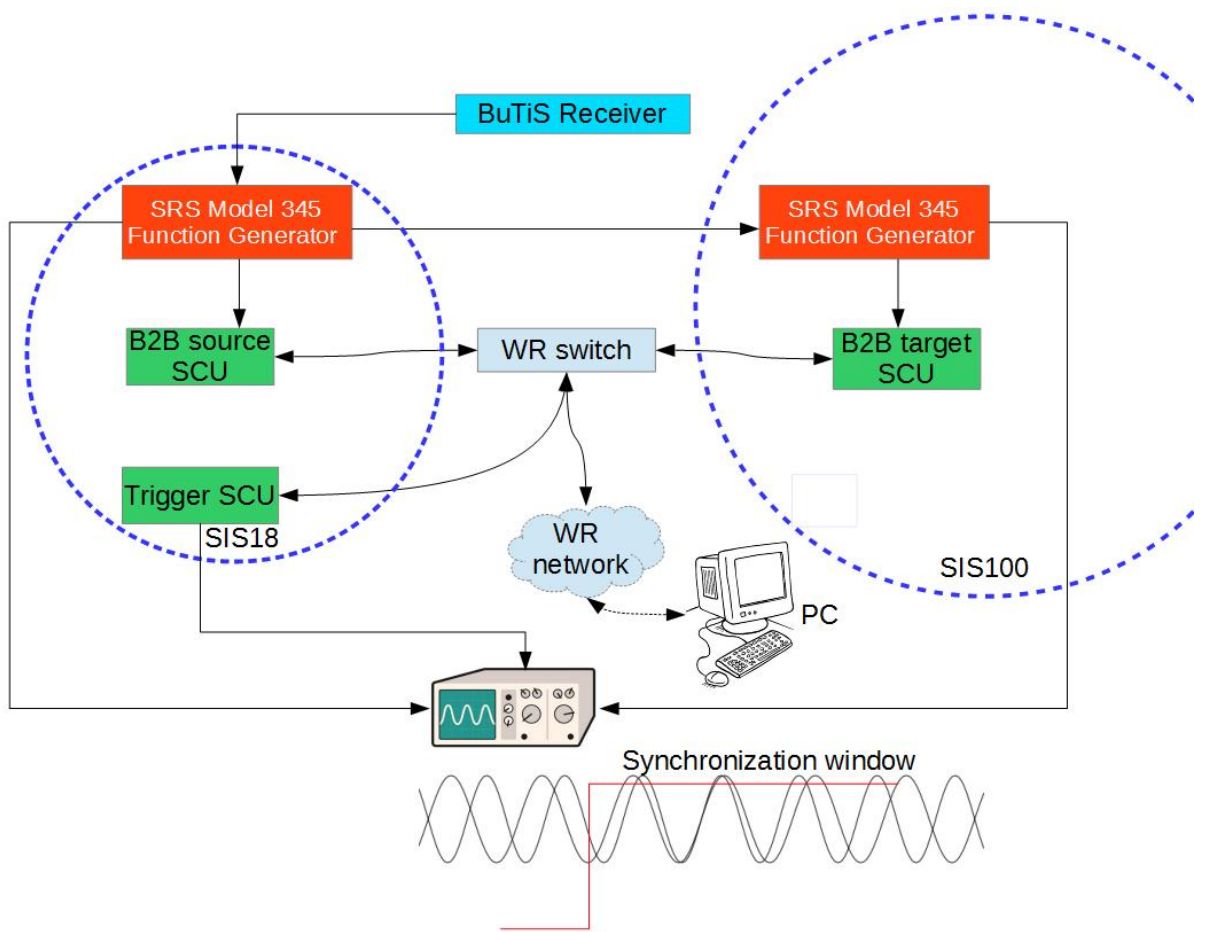


Abbildung 5.14: Schematic of the test setup

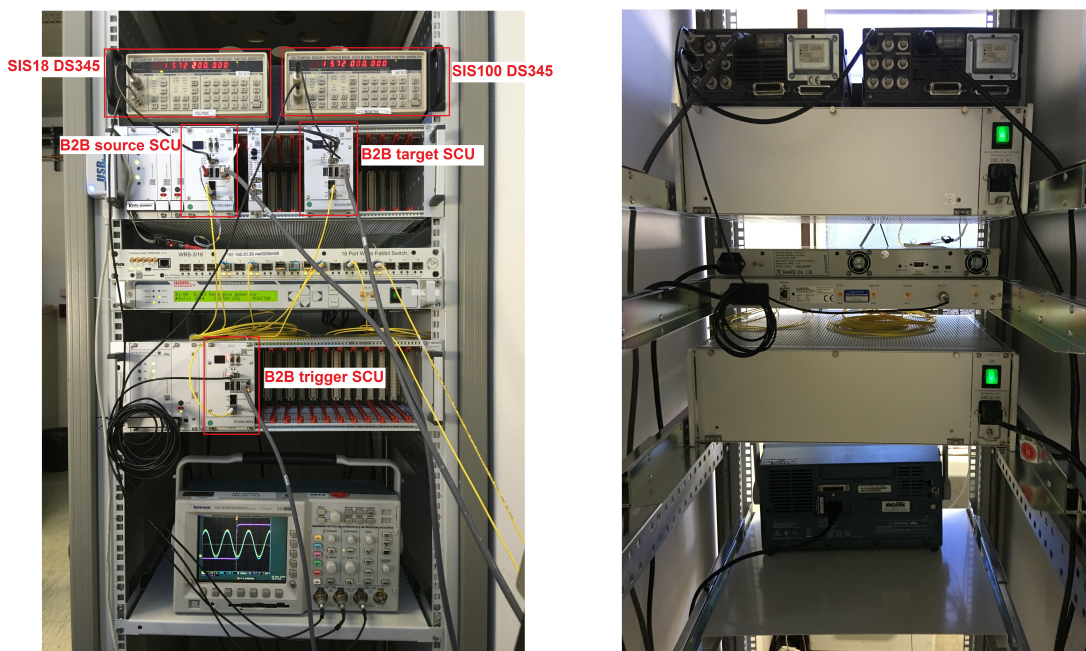


Abbildung 5.15: Test setup

Fig. 5.16 shows the flow chart of the B2B programs running on the soft CPU LM32 of the B2B source.

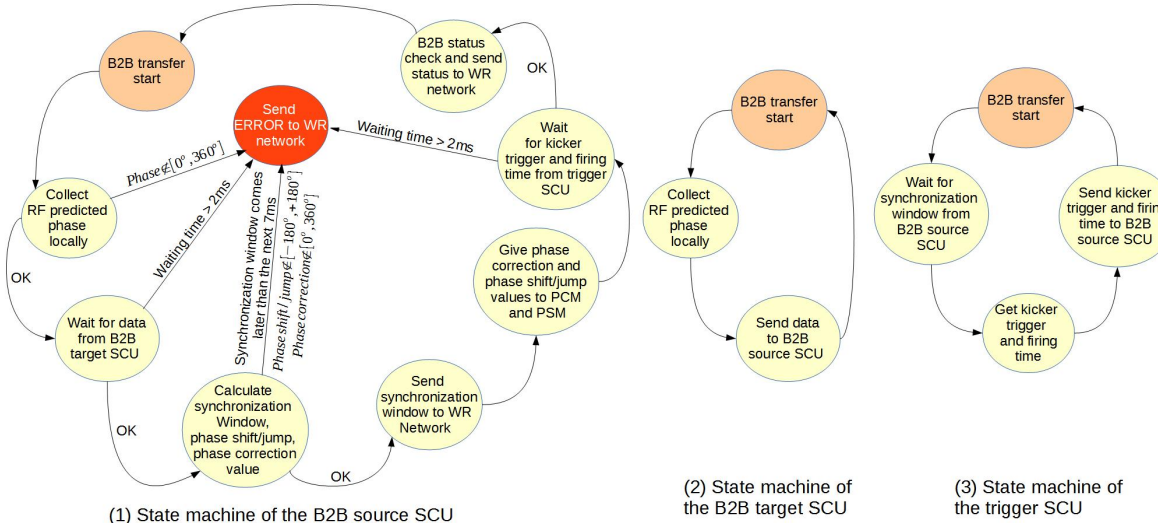


Abbildung 5.16: Flow chart of the B2B programs on SCUs.

Übersicht über SG an GSI, Aufbau, Funktionsweise

5.4.3 Test result

Fig. 5.17 shows status of the B2B programs on SCUs of the test setup.

Abbildung 5.17: The result of the test setup

Fig. 5.18 shows part of the SCU layout. The B2B event queue gets the B2B related telegrams at their absolute execution time. The timestamp zero-crossing points module is used to get the timestamp of the zero crossing point of the DS345 sine wave. The latching of the timestamp is triggered by LM32. The SCU slave interface supports the write and read between the LM23 and SCU slaves. LM32 of the B2B source and target SCUs are polling their B2B event queues. When they get

the B2B start event, they trigger the timestamp zero-crossing points module to latch timestamp. The asynchronous trigger is because of not only the non-real time of the program running on LM32, but also the block of the wishbone bus between top and dev crossbar by the monitor applications. So the B2B source and target SCU do not get the timestamp of the adjacent zero crossing points of two RF simulated sine signals in Fig. 5.17. In the test, the difference between two timestamps is 41.296us. The difference between timestamps of the adjacent zero crossing points, 592us, is the remainder resulting from 41.296us dividing SIS18 revolution period 636051ps. Based on the equation A and B, we could get the number of the SIS18 revolution period 3634 and the synchronization time 4.622818ms. For the real B2B transfer system, LM32 read the predicted phase from the PAP module when it polls the B2B start event. Only LM32 is allowed to use the wishbone bus between top and dev crossbars. The asynchronous reading is only caused by the non-real time LM32 program, which is around 1us. For the PAP module, the predicted phase is constant for 9us.

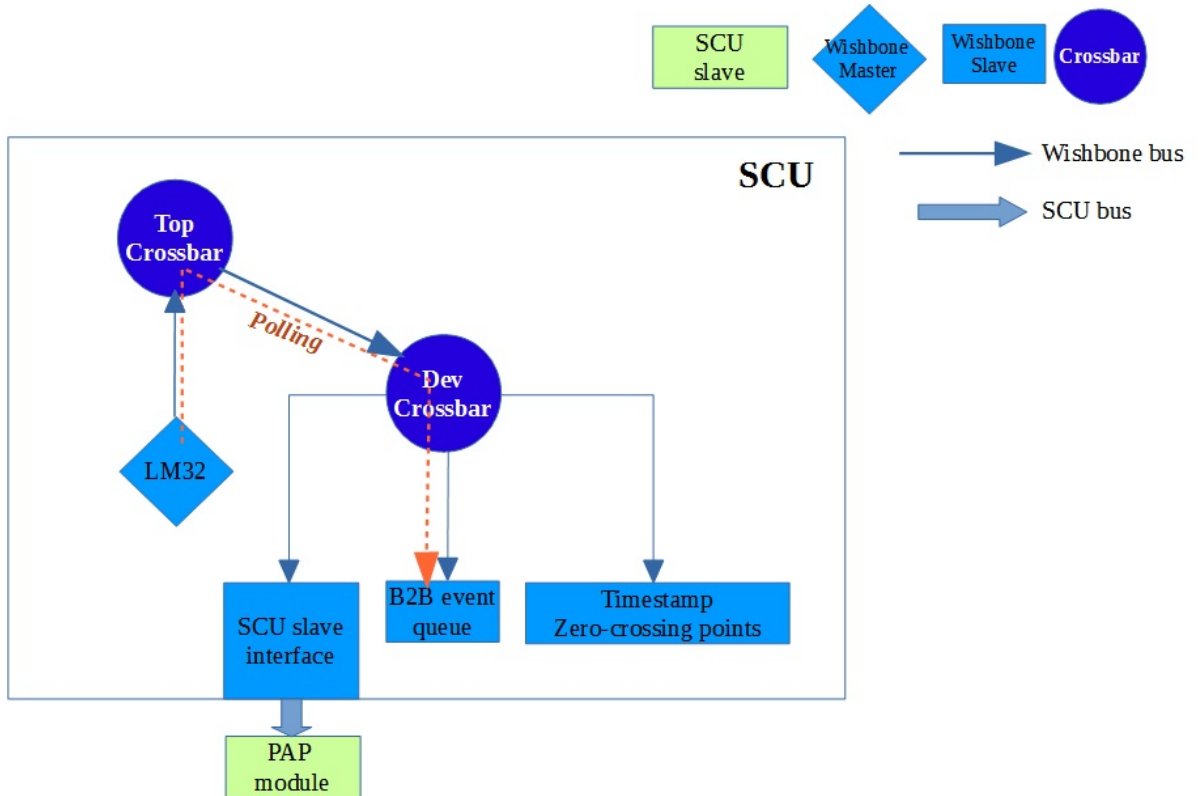


Abbildung 5.18: Topology of the SCU.

Kapitel 6

Existing transfer system and the transfer system of the FAIR accelerators

- 6.1 Existing transfer from SIS18 to ESR
- 6.2 B2B transfer from SIS18 to ESR to CRY-RING

Kapitel 7

Summary

Kapitel 8

Acknowledgement

I wish to express my sincere gratitude to Prof. Oliver Kester, David Ondreka and Dietrich Beck for their supervision, valuable guidance and helpful suggestions. I would like to express my sincere appreciation to Turgut «elikadam, for providing us VoIP device for our measurements. He also helped us for adding extra functions for delay measurements to VoIP device. And also I want to thank to Hasan «itÁ and my friends in ASELSAN Inc. for their valuable friendship, help and support. I want to thank to Şanser Şirin from Hacettepe University and Oktay KoÁ from Middle East Technical University for their help and support during measurements. And also I want to thank to Mehmet Celep, Alparslan G^zel and Halil İbrahim Seyrek from Gebze Institute of Technology for their help and support during measurements. I am also grateful to ASELSAN Inc. for facilities provided for the completion of this thesis. I am grateful to my wife, Esin, because she always supported me and cheered me up when I needed.

Kapitel 9

References

Literaturverzeichnis

- [1] D. Beck, R. Bär, M. Kreider, C. Prados, S. Rauch, W. Terpstra and M. Zweig , *THE NEW WHITE RABBIT BASED TIMING SYSTEM FOR THE FAIR FACILITY*, PCaPAC'12, India, p. 242, (2012)
- [2] D. Beck, *Interface to BuTiS*, <https://www-acc.gsi.de/wiki/Timing/TimingSystemButisInterface>
- [3] C. Bovet et al., *A Selection of Formulae and Data Useful for the Design of A.G. Synchrotrons*, rev. version, CERN-MPS-SI-INT-DL-70-4 (CERN, April 23, 1970)
- [4] P. Moritz, *BuTiS - Development of a Bunchphase Timing System*, GSI Scientific Report 2006, p. 64, (2007)
- [5] G. Dugan, *Considerations of BunchSpacing Options for Multi-Bunch Operation of the Tevatron Collider*, Fermi National Accelerator Laboratory, p. 1, (1989)
- [6] D. Ondreka, *Settings Generation for the RF Systems in FAIR*, GSI/CERN Meeting 2014
- [7] H. Liebermann, D. Ondreka, *FAIR and GSI Reference Cycles for SIS18*, GSI, October 3, 2013
- [8] Eizi EZURA, Masahito YOSHII, *BEAM-DYNAMICS VIEW OF RF PHASE ADJUSTMENT FOR SYNCHRONIZING J-PARC RCS WITH MR*, High Energy Accelerator Research Organization, Japan, June, 2008
- [9] John R. Taylor, *AN INTRODUCTION TO Error Analysis* University Science Books, Sausalito, California, 1997
- [10] H Liebermann, D. Ondreka, *FAIR and GSI Reference Cycles for SIS18 Primary Beams - System Planning*, Sausalito, GSI, 2013
- [11] Stanford Research Systems, *MODEL DS345 Synthesized Function Generator*
- [12] H. Klingbeil, *Low-Level-RF (LLRF) Systems for FAIR Synchrotron and Storage Ring Cavities*, FAIR-Technikforum, November.11.2010
- [13] S.Y.Lee, *Accelerator Physics*, Third Edition.PP.241-243,2012